UNIVERSITY OF CALIFORNIA SAN DIEGO

Characterizing the interactions between Influenza A virus NS1 and the mRNA•eIF4E•eIF4G1 Complex

A Thesis submitted in partial satisfaction of the requirements for the degree
Master of Science

in

Chemistry

by

Alejandro Cruz

Committee in charge:

Professor Simpson Joseph, Chair
Professor Gourisankar Ghosh
Professor Colleen McHugh

2022

The Thesis of Alejandro Cruz is approved, and it is acceptable in quality and form for publication on microfilm and electronically.

University of California San Diego

2022

TABLE OF CONTENTS

LIST OF FIGURES

ACKNOWLEDGEMENTS

I am incredibly thankful for various opportunities Dr. Simpson Joseph has given me throughout my scientific career. From Allowing me to first work as an undergraduate researcher to re-joining his lab as a M.S. student. As a mentor, he has taught me a lot about how to conduct experiments diligently, purposefully, and attentively. He has been an amazing mentor, stern and straightforward but understanding when needed. In addition to Dr. Joseph, I'd like to thank the Joseph lab in its entirety. The lab members have watched me develop into the graduate student I am today, and I can confidently say I would not be the researcher I am today without their advice.

Finally, I'd like to thank my mother, girlfriend, family, and friends. Without their constant support and distractions, I would not have been able to succeed in graduate school. They celebrated my successes while comforting me through the failures. I am indebted to each and every single one of you. Thank you.

ABSTRACT OF THE THESIS

Characterizing the interactions between Influenza A virus NS1 and the mRNA•eIF4E•eIF4G1 Complex

by

Alejandro Cruz

Master of Science in Chemistry

University of California San Diego, 2022

Professor Simpson Joseph, Chair

The annual epidemics caused by the influenza A virus causes hundreds of thousands of deaths worldwide. The non-structural protein of the influenza A virus, NS1, is the main antagonist of the host immune response which assists in the proliferation and virulence of the virus. NS1 is important for preventing nuclear export of host mRNA into the cytoplasm, avoiding activation of the viral RNA sensor RIG-I and the stimulation of mRNA translation. Despite being extensively studied, NS1's ability to influence the host's translational machinery is

not yet understood. However, previous studies have shown NS1 is able to interact with the eukaryotic translation initiation factor 4G (eIF4G) and poly(A)-binding protein 1 (PABP1), two proteins crucial to the translation initiation process.

Here we directly measured the NS1 and eIF4G interaction in the context of the 5'-m^7G-mRNA•eIF4E•eIF4G1 complex. Our results indicate NS1 is able to bind this complex both in the presence and absence of 5'-m^7G-mRNA. Similarly, our experiment show NS1 can bind eIF4E but only in the absence of 5'-m^7G-mRNA. In conjunction with previously reported data detailing NS1's ability to bind the 40S ribosomal subunit, we hypothesize NS1 stimulates translation by facilitating the interaction between the 5'-m^7G-mRNA•eIF4E•eIF4G1 complex and 40S-containing pre-translation initiation complex through a network of interactions.

Chapter 1: Introduction

1.1 Characterization of Influenza Virus and Human Virulence

Influenza is a contagious respiratory disease that is caused by influenza viruses. The most common of the influenza viruses to affect humans are described as the influenza virus type A (IAV) and the influenza virus type B. IAV is the most prolific among the two in its infection rate in humans, due in part to IAV's circulation in the human population as a recurring seasonal epidemic illness[1]. However, humans are not the main reservoir of IAV as a majority of the subtypes of IAV are naturally found circulating in wild aquatic birds[2]. Through a process known as genetic reassortment, IAVs have been documented in their ability to infect mammals aside from humans. Different strains of the virus have been found in populations of swine, horses, dogs and bats, highlighting their versatile host range[3]. Oftentimes multi-host strains allow for major interspecies infections, resulting in extremely pathogenic strains as was the case for the 1918 IAV pandemic. Dubbed the "Spanish Flu", there were noticeable similarities between the "classical" swine flu (isolated from swine in 1930 and from humans in 1933) and the 1918 strain, suggesting it originated in the wild waterfowl population but directly or indirectly adapted to infect humans[4]. The Spanish flu was perhaps the deadliest strain in recent human history, with an infection rate of .5% to 1% in the United States but totaling an estimated 50 million to 100 million deaths worldwide in the first pandemic year[4,5].

IAV continues to infect 9.2 to 35.6 million in the United States alone[6]. Of which, 114,000 to 633,000 lead to hospitalizations and 16,000 to 76,000 result in death[6,7]. Consequently, the United States is burdened annually with an estimated $11.2 billion cost to the health care system

and society as a whole[8,9]. Globally, seasonal IAV accounts for between 291,243 to 645,832 deaths annually with developing countries most affected[10].

IAV infection is characterized by the sudden onset of high fever, coryza, cough, headache, prostration, malaise, and inflammation of the upper respiratory tree and trachea[11]. Complications caused by IAV include pneumonia and acute respiratory failure, with serious viral infection complications including cardiac failure, renal failure, and hypoxemia[1,12]. The host becomes infectious in the first three days to four days of becoming symptomatic, but symptoms can persist for up to two weeks[13]. The contagion is spread through talking, sneezing, and coughing or through physical contact with contaminated surfaces. Clinical studies show the infectivity of IAV is relatively high, believed to only require a few viral particles, but the usage of a facial mask has been shown to dramatically hinder the transmission throughout the susceptible population[14]. The use of vaccines is perhaps the single most effective method in preventing the populous spread of IAV. Major vaccination has been shown to reduce the risk for IAV related illness, hospitalization, and serious infection outcomes that lead to death[15]. There are three distinct types of IAV vaccines, the inactivated influenza vaccine, the recombinant influenza vaccine, and the live attenuated influenza vaccine[16]. Because it is difficult to attempt to predict which strain of IAV will circulate, seasonal influenza vaccines are trivalent and formulated to contain the strains most likely to appear in the forthcoming season[17].

1.2 Architecture of Influenza A Virus

Influenza A virus (IAV) belongs to segmented, negative-sense RNA family *Orthomyxoviridae* and genera *Alphainfluenzavirus*[18]. IAVs are distinct from their influenza B

and influence C viruses in that the nucleoprotein (NP) and matrix protein (M1) are distinctly different[19]. IAVs are further categorized by the subtypes of their surface glycoproteins, the hemagglutinin (HA) and the neuraminidase (NA), there are distinct genetic subtypes for each glycoprotein, 16 for HA and 9 for NA[19]. The genome consists of eight unique segments of single-stranded, negative-sense RNA which encode for 10 viral proteins: HA, NP, NA, PB1 polymerase subunit (PB1), PB2 polymerase subunit (PB2), PA polymerase subunit (PA), matrix protein 1 (M1), matrix protein 2 (M2), non-structural protein 1 (NS1) and nuclear export protein (NEP)[20–22].

The HA and NA glycoproteins are found on the surface of the lipid membrane. HA allows for entry into the host cell, while NA allows for the release from the infected cell and the M1 and M2 proteins form the virion nucleocapsids, underneath the virion envelope[20,23]. HA binds the sialic acid on the host cell, while NA destroys and removes the sialic acid allowing for the host and viral glycoproteins to merge[24]. Then the HA glycoproteins allow the uptake of the viral particle into the cell and early endosome[18,25]. Following the completion of the uncoating process, the viral ribonucleoproteins (RNP) complexes, viral RNA (vRNA) coated in multiple NPs, are released into the cytoplasm and imported into the nucleus[26].

The PB1, PB2 and PA form the heterotrimeric viral RNA-dependent RNA polymerase. In regard to synthesizing mRNA from negative-sense vRNA, the polymerase binds the 5’ end of the template vRNA while simultaneously interacting with the 3’ end in order for polyadenylation to take place[27]. The RNA polymerase synthesizes the poly(A) tail of IAV mRNAs by reiterative copying of the U track in the vRNA[28,29]. Poly-(A) tailed modification has been shown to enhance translation in eukaryotic systems, this modification may help IAV deceive the host into translating viral mRNA[30].

Following successful translation of viral proteins, the multiple NA and HA are targeted to host lipid rafts, causing enlargement and recruitment of the M1 protein[31]. NEP mediates the nuclear exportation of viral ribonucleoprotein (RNP) complexes[19,21]. As M1 binds the glycoprotein-lipid multiplex, it serves to dock the viral RNPs and may mediate the addition of the M2 protein[31]. The viral RNA is then packaged and incorporated into the forming virus[19]. Then M2 protein alters the membrane, allowing for the scissoring and release of the progeny virion[31]. The newly formed virus particles have been shown to contain host-cell proteins within the virion, often associated with host lipid rafts, but their function has yet to be determined[32].

Of all the viral proteins IAV produces, NS1 is the only viral protein absent in the final virion. Generally, NS1 is divided into two distinct domains separated by a linker region (LR), the RNA-binding domain (RBD), effector domain (ED) and a disordered "tail" region (Figure 1.1)[33,34].

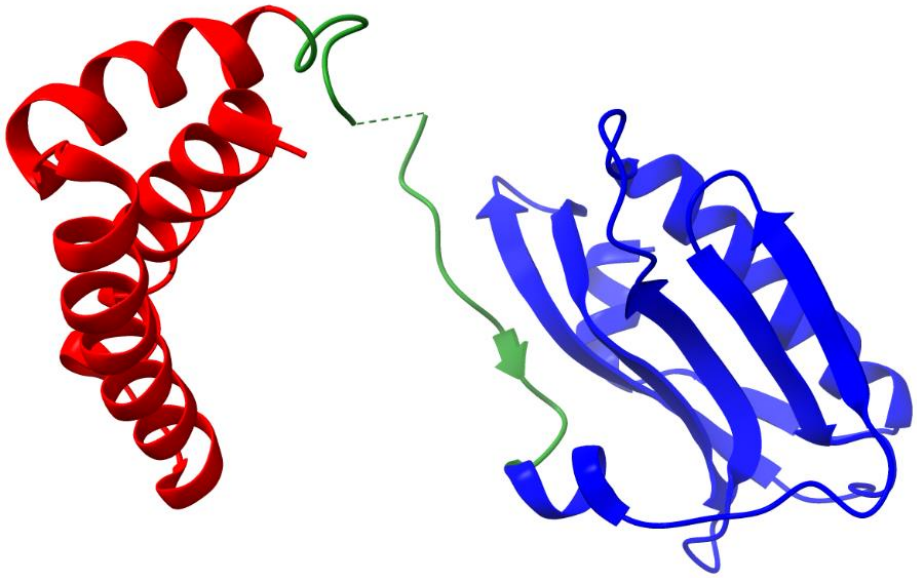

Figure 1.1: Structure of NS1 from H5N1 Influenza A Virus. Structure of the H5N1 NS1 with the individual domains identified by color, resolved by x-ray crystallography. The N-terminal RNA binding domain (Red), Linker Region (Green) and C-terminal effector domain (Blue). Protein Data Base Code: 3F5T.

A recent structure of NS1 has illustrated not only the dimeric interactions between each pair of RBD and ED, but the aforementioned interactions result in the formation of a chain-like structure instead of single dimers (Figure 1.2)[34–36]. Similar domain-domain interactions have also been observed in the only other structure of an NS1variant belonging to the H6N6 IAV[37]. This cooperative binding appears to be significant in all strains of NS1 and may aid in sequestering important molecular factors that enhance IAV's ability to antagonize the immune response. In addition, a recent study looked into the differences between subcellular localization of NS1 containing a mutation in the LR versus wildtype NS1 and found the LR is critical for the localization of the NS1 protein, in turn affecting its antiviral function[38].

The amino acid sequences across multiple, distinct NS1s from different IAV strains share relatively similar sequence identities. The NS1 from H3N2 has 66.96% similarity with the NS1 from the H5N1, while sharing 91.30% with H2N2's NS1. Additionally, H3N2's NS1 has 84.78% similarity with H1N1's NS1 and 76.04% with the H7N9 NS1[39]. Substantial sequence variations occur in the C-terminal region of the ED, implying this region is of less importance in regard to NS1's function. In addition, the variability between LR length does not seem to determine NS1's flexibility, as the NS1 containing a deletion in the LR (H5N1) was able to adopt similar open/close confirmations comparative to the NS1 with a longer LR region (H6N6)[40].

A

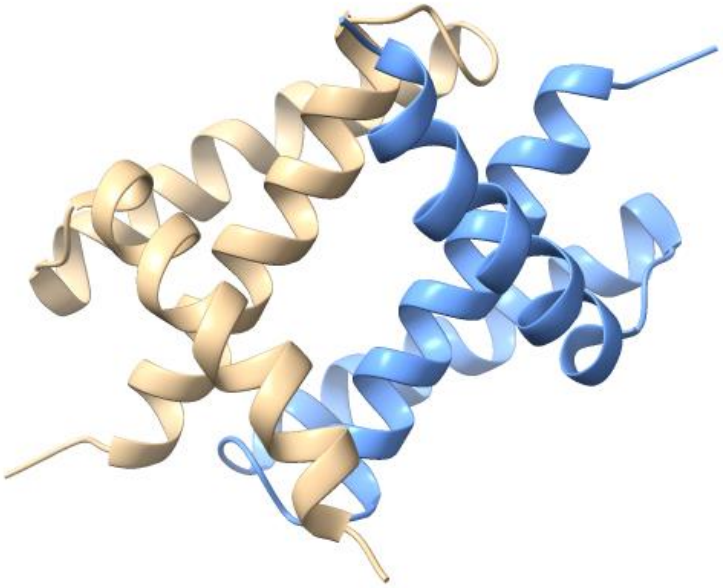

B

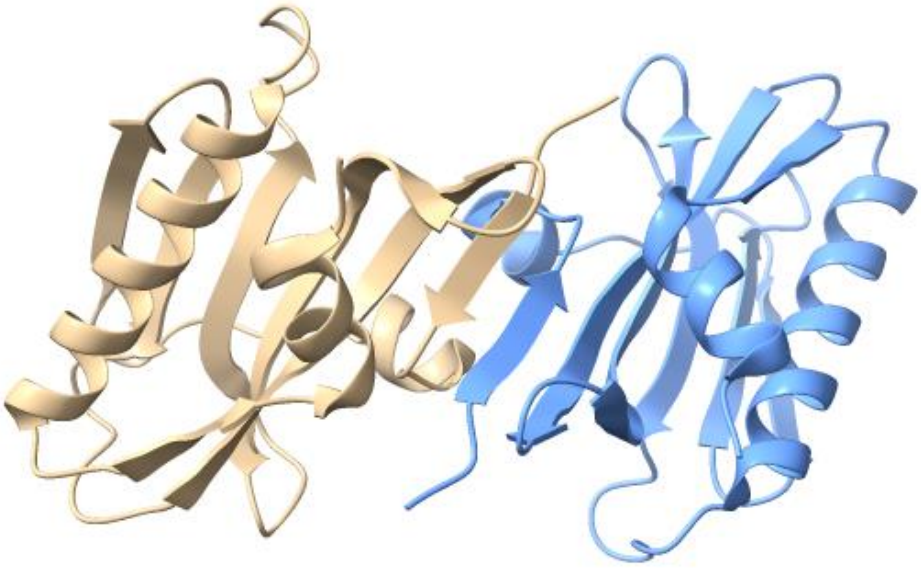

Figure 1.2: Structure of the dimerized RNA binding domain of H1N1 NS1 and structure of the dimerized Effector domain of H1N1 NS1. (A) Dimerization interface of two RNA binding domains, resolved through solution NMR. (B) Dimerization interface of two Effector domains, resolved through x-ray crystallography. Protein Data Base codes; RNA binding domain: 2N74, Effector domain: 6DGK.

1.3 IAV and the Human Immune Response

There are various documented strategies implemented by the influenza A virus (IAV) to actively avoid triggering the immune response of the infected host cell. When IAV enters the cell stimulus-specific signals are transduced throughout the interferon pathway where pattern recognition receptors activate interferon genes[41]. IAV's non-structural protein (NS1) is the main antagonist of the host immune response, it is a key player in multiple immune evasion strategies implemented by IAV. Evidence strongly suggests this is NS1's main role regarding IAV's success in host infection. As one study demonstrated, an NS1 deficient IAV was still able to proliferate in Vero cell lines, a cell line lacking type 1 interferon (IFN) expression[42]. In contrast, the same NS1 deficient IAV was shown to have its reproducibility greatly hindered while infecting IFN-competent cell lines.

NS1 has been documented in binding molecular targets that are essential to IFN production and initiation. The cleavage and polyadenylation specificity factor (CPSF) 30, of the CPSF complex, is one such molecular target. NS1 binds CPSF30, preventing the processing of the 3'-end of IFN-β pre-mRNA and other cellular pre-mRNA[43–45]. This is significant as RNA viruses such as IAV stimulate the activation of the RIG-1 RNA helicase, which leads to the formation of IFN-β pre-mRNA. By inhibiting the CPSF complex from processing the IFN-β pre mRNA, IAV can effectively negate the RIG-1 RNA helicase-induced IFN response. NS1's ability to bind CSPF30 is essential for efficient replication of IAV[45]. In addition to this, NS1 also interacts with both poly(A)-binding protein I and II (PABPI and PABPII) of the cellular 3'-end processing machinery[46–48]. This binding of NS1 to PABPI and PABPII inhibits the 3'cleavage of the pre-mRNA, which in turn prevents the poly(A) polymerase catalyzed synthesis of long poly(A) tails[47,49]. Stopping the nuclear export of mRNA into the cytoplasm, as poly(A) tails are

used by eukaryotic organisms to promote translation of the mRNAs[30]. In addition to stopping the processing of pre-mRNA with CPSF30, NS1 adds another level of interference regarding the translation of the antiviral host defense IFN.

NS1 also targets the ubiquitin ligase TRIM25 in an effort to stifle a host immune response by avoiding detection of the viral RNA sensor RIG-I and its facilitation of IFN production (Figure 1.3)[50]. This is done by binding to the coiled-coil domain of TRIM25, resulting in a blockage of TRIM25 multimerization which then disables TRIM25's ability to ubiquitinate the CARD domain of RIG-1[51]. This TRIM25 binding site was mapped to two amino acids of NS1 essential for this interaction, E96 and E97.

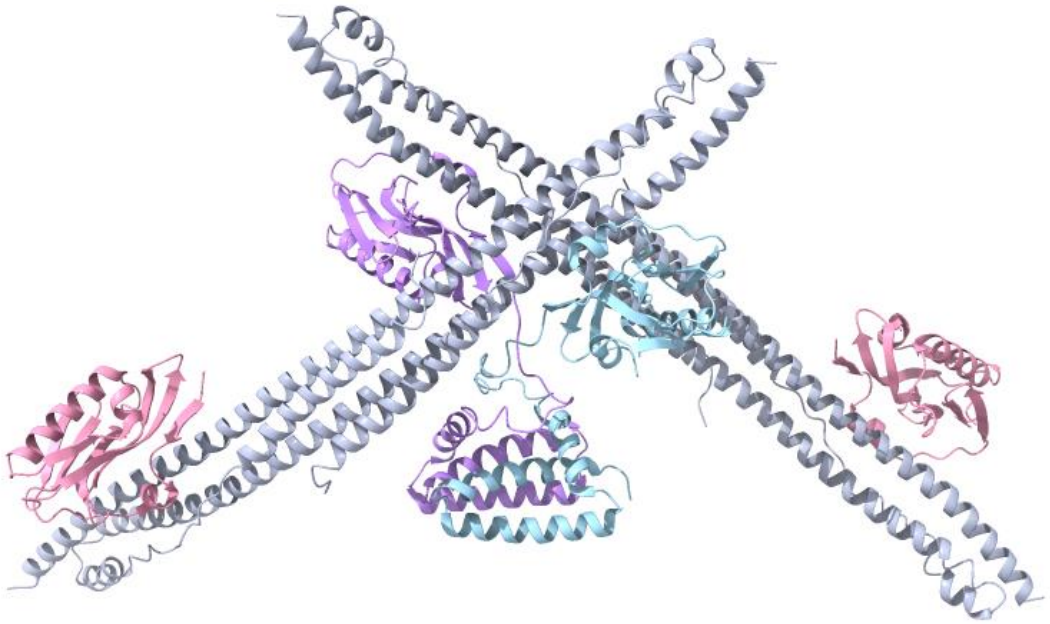

Figure 1.3: Structure of the Complex of H1N1 NS1 with the coiled coil domain of TRIM25. Binding interface of the TRIM25 domain (Grey) and the effector domain of NS1 (Purple and Teal), resolved through x-ray crystallography. Protein Data Base code: 5NT2.

One target of NS1 is the NLR Family Pyrin Domain Containing 3 (NLRP3) inflammasome, an essential part of the host's innate immune response. NS1 efficiently decreased the secretion of both pro-inflammatory cytokines, IL-1β and IL-18, by impairing the transcription of the nuclear factor κB. In addition, NS1 interacts with the endogenous NLRP3, leading to strong inhibition of the NLRP3 inflammasome[52].

In addition to binding molecular factors to stall the host IFN response, NS1also directly binds the export receptor NXF1•NXT1, the principal receptor mediating the docking and translocation of mRNAs through the nuclear pore complex[53]. By occupying the nucleoporin binding site on NXF1•NXT1, NS1 effectively prevents NXF1•NXT1 from escorting host mRNAs through the nuclear pore complex.

IAV has been shown to possess both anti-apoptotic and pro-apoptotic functions, utilizing both to allow sufficient time to replicate and produce viral proteins in which the virus can induce apoptosis and release the virion to neighboring cells. The anti-apoptotic nature is derived from NS1's ability to up-regulate Phosphatidylinositol 3-Kinase (PI3K)[54]. NS1 has been shown to significantly increase of p85β-associated PI3K activity when bound to the p85β regulatory subunit of PI3K[55,56]. The direct binding of NS1 to p85β is mediated by the effector domain of NS1 and the iSH2 domain of p85β[57–59]. IAV with a y89f mutation was seen exhibiting stunted growth, suggesting this signaling pathway is essential for competent virus reproduction[59]. NS1's influence on the p53 induced apoptosis is not yet fully understood. Despite evidence of NS1 and p53 colocalization, one study found there was not significant IAV-caused apoptosis in HeLa cells to draw any conclusions[60]. Another study noted an increase in inhibition of p53-mediated transcriptional activity and apoptosis caused by NS1 interaction[61]. In contrast, NS1 has also been shown to stabilize p53 but only modestly modulates p53's transcriptional activity[62]. While a

more recent publication by the same group demonstrated E3-ubiquitin ligase Mdm2 was destabilized by NS1 and in turn affecting the p53/Mdm2 interaction and regulatory loop during the time-course of infection[63]. Though uncertain to what extent, NS1 is an important player in IAV's command over the regulation of the host cell cycle.

1.4 NS1 and Influence over Host Translation

The RNA binding domain (RBD) of NS1 binds both single stranded RNA (ssRNA) and double stranded RNA (dsRNA), both of which have heavy implications on regulation operating at multiple post-transcriptional steps[64,65].The RBD forms a homodimer complex with dsRNA through substantial hydrogen bonding, in which the Arg38 pair is instrumental in dsRNA binding in vivo[66]. This proves useful for IAV as NS1's ability to bind dsRNA assists in sequestering the viral RNA (vRNA) from the host immunity, preventing the interferon cascade[67]. Although no direct correlation has yet been determined, this binding of viral mRNAs paired with NS1's interaction with the viral transcription-replication complexes, suggest NS1 plays a role in late stage transcription and replication[68]. In addition, NS1 has been determined to be a poly(A)-binding protein that impedes the nuclear export of mRNA containing poly(A) tails[69]. This nuclear retention of mRNA prevents the host cell from translating its own proteins, anti-viral and conventional[70].

In a seemingly contradictory fashion, NS1 has also been documented in stimulating translation initiation of viral mRNAs. One study found when NS1 was co-expressed with virus nucleoprotein (NP), an enhancement of NP translation was observed along with NS1 association with the host polysomes[71]. Furthermore, translational stimulation of the M1 protein by NS1 has

also been documented[72,73]. Though still unclear, the preferential translation of viral mRNAs has much to do with the 5' untranslated region (5'-UTR) of vRNA. As NS1 has been observed binding the 5'-UTRs of mRNAs coding for IAV M1, NP and NS proteins[73–75].

Interestingly enough, one study demonstrated the N-terminal half of NS1, the RBD, is sufficient for both the nuclear retention of host mRNA and simultaneous enhancement of vRNA translation[76]. In addition, another study discovered this NS1 domain is essential for efficient synthesis for all viral proteins in infected cells[77]. Similarly, the RBD region has also been implicated in provided NS1's ability to associate with the 40S and 60S ribosomal subunits[78].

1.5 NS1, directly and indirectly, influences the Eukaryotic Translation Initiation Factors

Although not completely understood, the influenza A virus (IAV) has been shown to directly modulate the eukaryotic initiation factor complex through its various subunits. One method implemented by IAV is by use of the blocking of the autophosphorylation and activity of p68[79]. This decreased p68 function directly impacts the phosphorylation of the alpha subunit of eukaryotic initiation factor 2 (eIF2), leading to efficient translation of viral proteins[80].

In addition to inhibiting phosphorylation of eIF2, IAV is associated with significant dephosphorylation and inactivation of the eukaryotic initiation factor 4E (eIF4E) of the eukaryotic initiation factor 4F (eIF4F) complex. This reduction of phosphorylation of eIF4E leads to an extremely limited amount of active translation factors able to form the complex and initiation of translation[81]. This allows for significant shut-down of host cap-dependent translation, while viral translation is unaffected as eIF4E impairment does not affect viral protein output[82].

Of IAV's ability to influence the eIF4F complex through its individual subunits, perhaps one of the most important is the interaction between its non-structural protein (NS1) and eukaryotic initiation factor 4G (eIF4G). This interaction has been recorded in transfected cells, cells infected with IAV, and in vitro with purified proteins[83]. This association is mapped to the amino acid region 81 to 113 on NS1 and amino acids 157-550 on eIF4G (Figure 1.4)[47,84]. In contrast with eIF4E, IAV's infection is greatly hindered in experiments that knocked down eIF4G1 in cell lines[85]. Evidence for eIF4G's importance in the viral life cycle, implies viral translation is heavily dependent on NS1's interaction with this cornerstone piece of the eIF4F translation complex.

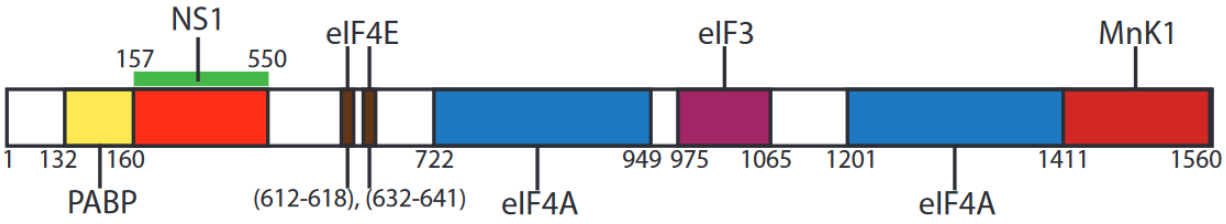

Figure 1.4: Architecture of human Eukaryotic translation initiation factor 4G. The amino acid sequences of the various binding partner of eIF4G. The red section denotes the amino acids that were previously shown to bind NS1.

Chapter 2: Investigation of NS1 binding to eIF4F subunits using fluorescence anisotropy and gel electrophoresis mobility shift.

Introduction

Aside from the broad range of amino acids involved, little is known about the binding interaction between non-structural protein (NS1) from Influenza A virus (IAV) and human eukaryotic translation initiation factor 4 G (eIF4G1). NS1 was first documented binding directly to eIF4G1 both in vivo and in vitro[83]. This was done using a series of overlay experiments, pull-down assays, and western blots. While qualitative, these experiments do not allow for a quantitative binding affinity to be determined. In addition, the studies previously performed were looking at this interaction in an isolated matter, without considering other pertinent biomolecules that may or may not influence the affinity of this interplay.

To better characterize this protein-protein interaction, we sought to describe the binding affinity qualitatively and quantitatively between a fluorescently labeled mutant of the NS1 protein of IAV and a shortened eIF4G1 construct. The NS1 construct forms both a monomer and dimer in solution, allowing us to investigate whether or not dimer formation affects this interaction. While the eIF4G construct contains the binding sites for poly(A)-binding protein I, eIF4E and NS1[83,86].

In chapter 2, we describe how we (1) purified and fluorescently labeled an NS1 mutant containing only the effector domain, (2) designed and purified a truncated human eIF4G, (3) designed and purified human eIF4E (4) quantified their binding affinity through a series of fluorescence anisotropy assays and gel electrophoresis mobility shift assays. These sets of experiments not only allow for a determination of dissociation constant but a visual

representation of this heterogeneous complex forming, all the while permitting complete control over the reaction conditions and supplemental biomolecules.

2.1 Designing, isolation, and fluorescein labeling of truncated NS1

The non-structural protein (NS1) from the A/Udorn/1972 (H3N2) strain was changed through PCR mutagenesis to have both the RNA-binding domain (RBD) (amino acids 1-80) and the linker region (LR) (amino acids 81-89) removed leaving only the effector domain (ED) (amino acids 89-207) and the disordered tail region (amino acids 208-237). The regions removed are known to be non-essential in NS1's ability to bind eIF4G[83]. Normally, the wildtype NS1 from H3N2 is a 26.8 kDa protein with 238 amino acids, while this mutant is only 17.9 kDa, with 157 amino acids in length. The removal of both the RBD and LR is largely in part to simplify and avoid protein purification complications while maintaining the residues necessary for the eIF4G1 interaction. NS1 is known to form multimeric chain-like complexes through the dimerization of the RBD and ED, causing solubility issues when purifying recombinantly[37]. In conjunction with avoiding purification issues, the NS1 (89-237) variant is small enough in size to observe a clear change in anisotropy when complexed with the eIF4G1 construct. In contrast, the wildtype NS1 might have been too large to notice any significant anisotropic change when complexed with eIF4G1.

This truncated NS1 was then cloned immediately downstream of an N-terminal hexahistidine tag for easy purification with immobilized nickel affinity chromatography following expression in an *E. coli* expression system. Following the purification of the NS1 (89-

237) variant, the protein was fluorescently labeled at the single cystine at amino acid position 116 with Fluorescein-5-Maleimide.

2.2 Designing and isolation of the eIF4G1 construct

The eIF4G1 constructed used for our experiments was designed and optimized by a former student. This eIF4G1 variant is 60.1 kDa protein containing amino acids 88 through 653 of wildtype eIF4G1. This mutant was first designed to study the translational complex formed by eIF4E•eIF4G•PABP1. It contained the binding sites for both eIF4E and PABP1 while maintaining the highest stability of all proposed variants analyzed by bioinformatic software ExPASy. Initially, this construct expressed very poorly in our recombinant expression system. To circumvent this issue, the sequence was codon optimized by GENEWIZ to maximize expression in *E. coli* systems. Following the success in increasing expression, the coding sequence for the eIF4G1 construct was cloned into a vector containing a C-terminal Mxe GyrA intein and a chitin binding domain. This sequence combination allowed for a self-cleaving C-terminal protein tag following isolation by way of chitin resin. This construct was further purified by size exclusion chromatography, resulting in a tag-less eIF4G1 construct with minimal contaminates.

2.3 Designing and Isolation of the eIF4E construct

The full length, wildtype of isoform 1 eIF4E. Spanning 217 amino acids, the cap-binding protein is roughly 25.0 kDa in size. This protein was first utilized to study the translational complex formed by eIF4E•eIF4G•PABP1. This protein's purification proved relatively

straightforward, utilizing the C-terminal hexahistidine tag, size exclusion chromatography and anion exchange chromatography. This recombinant protein retains at least two biologically relevant features of eIF4E, the ability to bind eIF4G1 and the ability to bind 7-methylguanosine capped mRNA. This eIF4E construct has been proven to successfully bind the aforementioned biomolecules in native conditions, as both a complex and individually.

2.4 Quantification of NS1 binding affinities to eIF4E and eIF4G1

The interaction between the effector domain (ED) of H3N2 IAV's NS1 and the eukaryotic translation initiation complex subunit 4G (eIF4G1) has only been characterized by the amino acid sequences. The article that initially reported this interaction found a construct containing amino acids 157 through 550 on eIF4G1 are sufficient to pull down NS1 in vitro[83]. In conjunction, the same article mapped the eIF4G1 binding site to the amino acids 82 through 113 on NS1. However, this study presented conflicting evidence as their pull-down experiment with their Δ1-81 construct showed no binding with eIF4G1 while the coimmunoprecipitated experiment with the same Δ1-81 construct demonstrated binding. Similarly, we were interested in exploring the possibility of NS1 binding eIF4E as NS1 has been previously shown to bind other translation initiation factors such as eIF4G1 and PABP1[47]. We sought to analyze protein-protein interaction in a more direct fashion by utilizing the change in anisotropy, avoiding the need for antibodies or pull-down experiments. We labeled the effector domain (amino acids 89 through 237) of the H3N2 NS1 protein with fluorescein on the cystine found on residue 116. We incubated the labeled NS1 (89-237) with increasing concentrations of either eIF4G1 (88-653) or eIF4E and measured the change in fluorescence anisotropy to quantify the equilibrium dissociation constant, K_D, for each interaction (Figure 2.4).

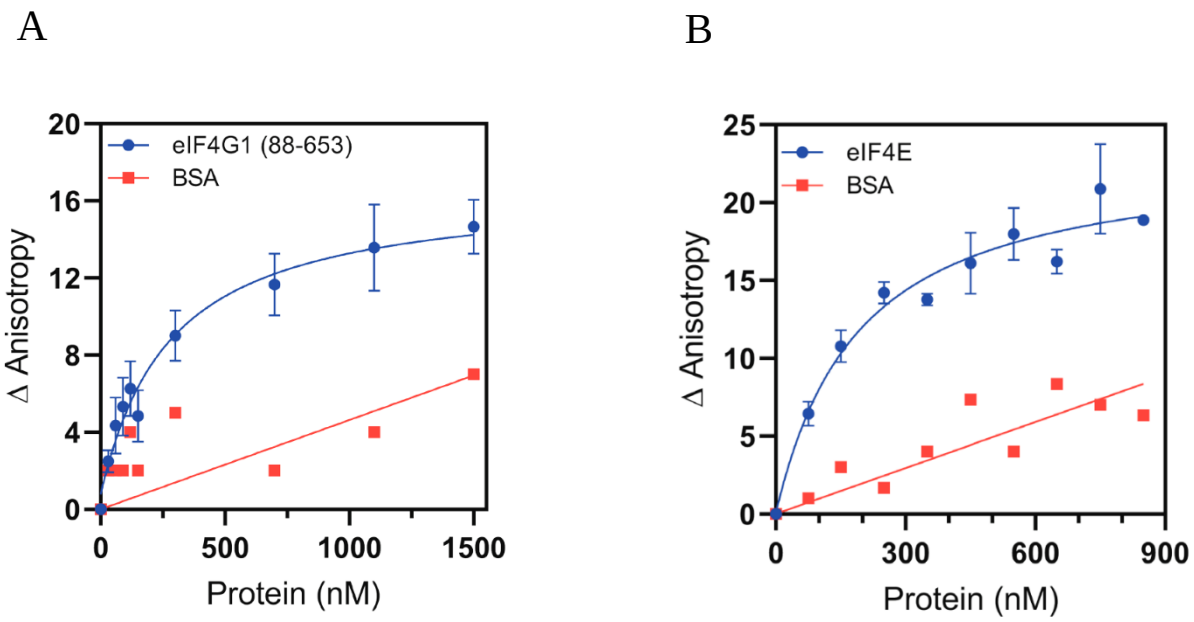

Figure 2.4: Binding curve graphs depicting the increase of fluorescence anisotropy of fluorescently labeled NS1 (89-237) caused by either eIF4G1 (88-653) or full-length eIF4E. (A) eIF4G1 (88-653) or Bovine serum albumin (BSA) titrated against 20 nM of NS1 (89-237)-FL. (B) eIF4E or BSA titrated against 20 nM of NS1 (89-237)-FL. BSA binding to NS1 (89-237)-FL was measured to test for non-specific interactions. The error bars show the standard deviations from three (eiF4E) or four (eIF4G) independent experiments.

We determined the K_D value for the NS1 and eIF4G1 (88-653) interaction was 264 ± 63 nM while the interaction between NS1 and eIF4E was demonstrated to have a value of 177 ± 39 nM. The strong affinity NS1 has for eIF4E was unexpected, as a previous study investigated NS1 binding to eIF4E but failed to confirm any interaction in vivo[83]. However, through our more direct method of measuring protein-protein interactions we were able to reveal and quantify the eIF4E/NS1 interaction, in addition to quantifying the already established eIF4G1/NS1 interaction.

2.5 Examining the various NS1 complexes with eIF4E and eIF4G1 in native gel conditions

Following our success with the anisotropy experiments, we wanted to be able to better visualize the fluorescein-labeled NS1 (89-237) interacting with eIF4E and eIF4G1 (88-653). Using an electrophoretic mobility shift assay (EMSA), we were able to visualize the formation of both the NS1•eIF4G(88-653) complex and the NS1•eIF4E complex under native conditions. We incubated a set concentration of fluorescein-labeled NS1 (89-237) with increasing amounts of either eIF4G(88-653) or eIF4E. Our results show a distinct band formation when fluorescein-labeled NS1 (89-237) is paired with either eIF4G(88-653) or eIF4E, indicating the formation of an NS1•eIF4G(88-653) complex and an NS1•eIF4E complex (Figure 2.5.1). Each EMSA was duplicated a total of three times to quantify the change of the relative intensity percentage from lane to lane.

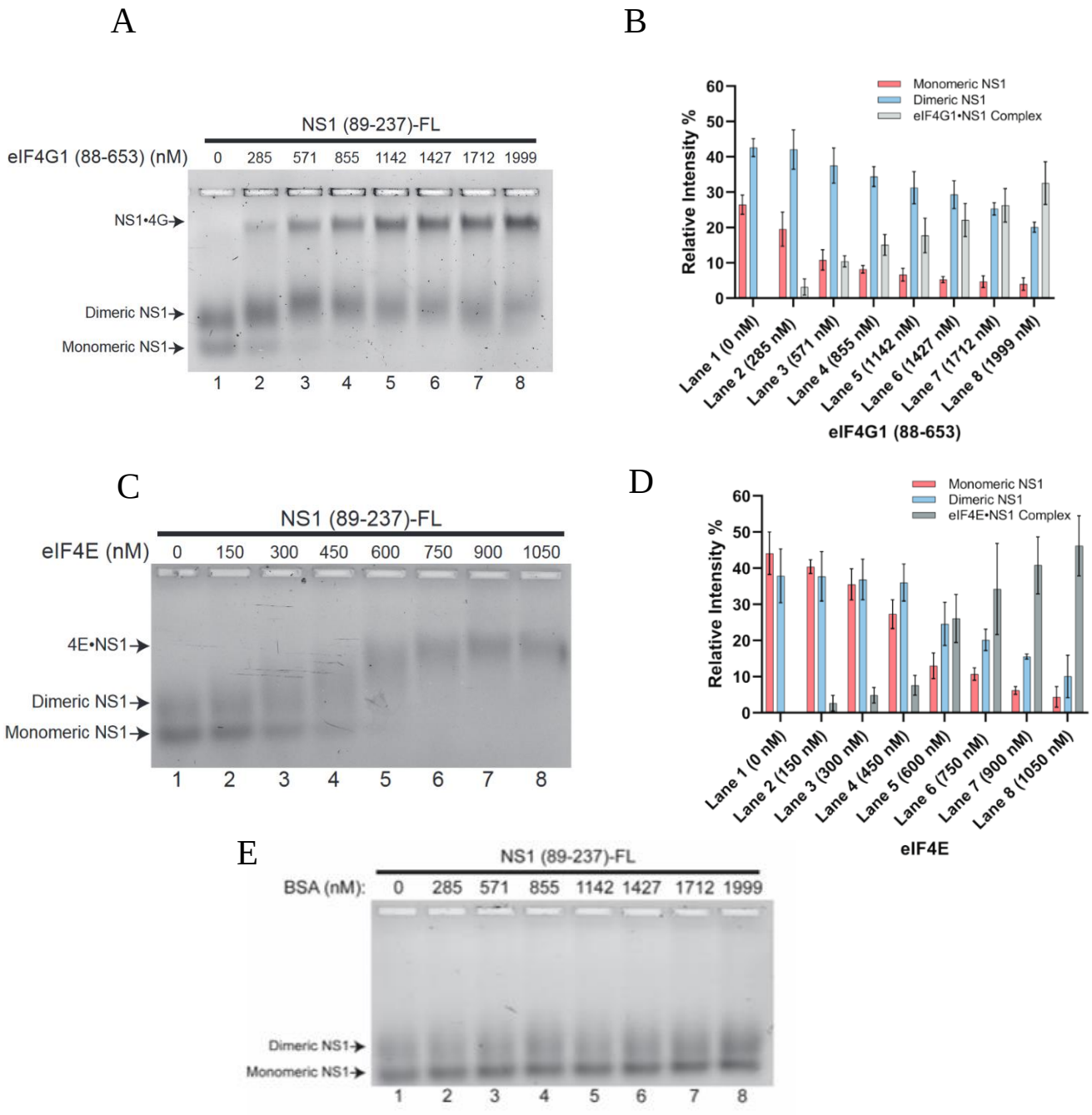

Figure 2.5.1: Electrophoretic mobility shift assay depicting the upward shift of fluorescently labeled NS1 (89-237) caused by either eIF4G1 (88-653) or full-length eIF4E. (A) eIF4G1 (88-653) was added in increasing amounts to 75 nM of NS1 (89-237)-FL, causing a shift and formation of a NS1•eIF4G band. (B) Quantification of the band intensities caused by the addition of eIF4G. The error bars depict the standard deviations from three independent experiments. (C) eIF4E was added in increasing amounts to 75 nM of NS1 (89-237)-FL, causing a shift and formation of a NS1•eIF4E band. (D) Quantification of the band intensities caused by the addition of eIF4E. The error bars depict the standard deviations from three independent experiments. (E) BSA was added in increasing amounts to 75 nM of NS1(89-237) to test for non-specific protein-protein interactions.

In hopes of further describing the NS1•eIF4E complex, we wanted to investigate whether this interaction was maintained if eIF4E was bound to a 5′-7-methylguanosine (m^7G) capped RNA. We formed the fluorescein-labeled NS1•eIF4E complex in the presence and absence of a 5′-m^7G-capped RNA. We discovered that the NS1•eIF4E complex is disrupted by the formation of the eIF4E•5′-m^7G capped RNA complex, as we observed an intensity decrease of the band corresponding to the NS1•eIF4E complex (Figure 2.5.2). Similarly, we attempted to observe the inverse interruption wherein the eIF4E is bound to 5′-m^7G capped RNA and the addition of excess NS1 leads to the intensity decrease of the band corresponding to the eIF4E•5′-m^7G capped RNA complex.

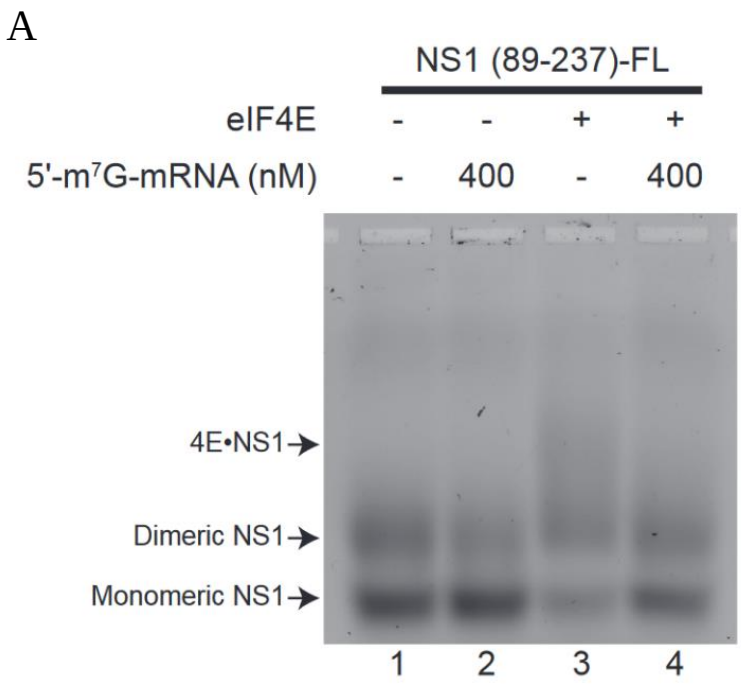

Figure 2.5.2: Electrophoretic mobility shift assay depicting the shifting from the fluorescently labeled NS1 (89-237)•eIF4E complex to the unbound NS1 (89-237) by 5'-m^7G-mRNA addition. (A) The NS1•4E complex was formed in the presence and absence of 5'-m^7G-mRNA. The concentration of NS1 was 75 nM.

Unfortunately, we were not able to successfully demonstrate this interruption, we theorize the high-affinity eIF4E has for the m^7G cap structure (60 nM) would require an overabundance of NS1 that was not feasible for our assay[87].

In addition to visualizing the separate complexes NS1 (89-237) forms with eIF4E or eIF4G (88-653), we were interested in determining how our NS1 (89-237) construct behaved when both eIF4E and eIF4G1 are present. We incubated fluorescein-labeled NS1 (89-237) with three different concentrations of eIF4G (88-653) in the absence and presence of a set concentration of eIF4E. We found that in the presence of both eIF4G and eIF4E, NS1 forms a single band distinct from either the eIF4G•NS1 complex or eIF4E•NS1 complex. This unique band pattern indicates NS1 prefers to form a single, unified complex with eIF4G and eIF4E instead of individual eIF4G•NS1 and eIF4E•NS1 complexes (Figure 2.5.3).

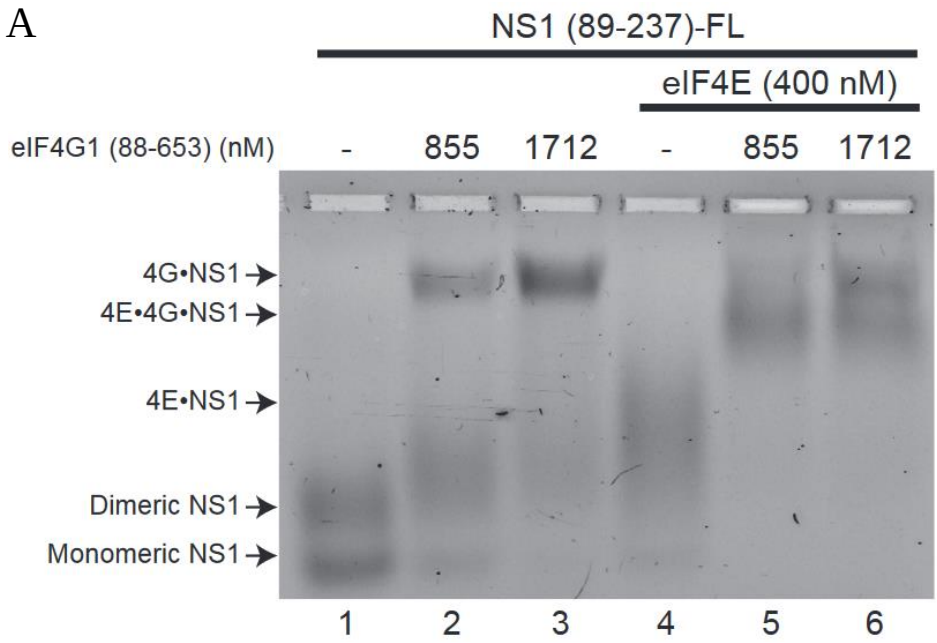

Figure 2.5.3: Electrophoretic mobility shift assay depicting the formation of the fluorescently labeled NS1 (89-237)•eIF4E•eIF4G complex. (A) In the presence of eIF4G and eIF4E, the NS1 band shifts upward and forms a single complex under the NS1•eIF4G band. The concentration of NS1 was 75 nM.

2.6 NS1 colocalizes with the 5′-m^{7}G-capped RNA bound eIF4E•eIF4G complex.

Finally, we were curious in answering whether or not NS1 (89-237) could bind the 5' m^{7}G-capped RNA•eIF4E•eIF4G complex. A previous study has shown that when eIF4E is complexed with eIF4G, eIF4E has a considerably high affinity for the m^{7}G capped structure[88]. Therefore, it would stand to reason that if eIF4E, eIF4G and a 5′-m^{7}G-capped RNA were in close proximity, as they would in the cytoplasm, they would form a single complex. For this reason, we sought to form the 5′-m^{7}G-capped RNA•eIF4E•eIF4G complex with a fluorescently labeled 5′-capped RNA in the presence of our NS1. Because our NS1 (89-237) mutant is labeled with fluorescein, we labeled our 5′-capped RNA at the 3′-end with the CF555 hydrazide fluorophore in order to individually track each labeled biomolecule. We incubated the 5'-m^{7}G-mRNA-CF555 with NS1 (89-237) or eIF4G (88-653) to ensure our 5'-m^{7}G-mRNA-CF555 was not non-specifically binding to either protein. We formed the 5'-m^{7}G-mRNA•eIF4E complex and the 5'-m^{7}G-mRNA•eIF4E•eIF4G(88-653) complex (with and without NS1 (89-237)), both visualized through the CF emission scan. We then imaged the gel using a fluorescein emission scan to visualize any shift the labeled NS1 (89-237) may have experienced. We found that in the presence of the mRNA•eIF4E•eIF4G complex, the NS1 (89-237)-FL band shifts upwards and overlaps with the CF-555 band corresponding to the complex (Figure 2.6.1). This overlap of band intensities is better depicted in the composite scan, where the red color corresponds to the CF-555 labeled 5'-m^{7}G-mRNA while the yellow color corresponds to the fluorescein-labeled NS1 (89-237) and the overlap between these two colors results in the orange hue.

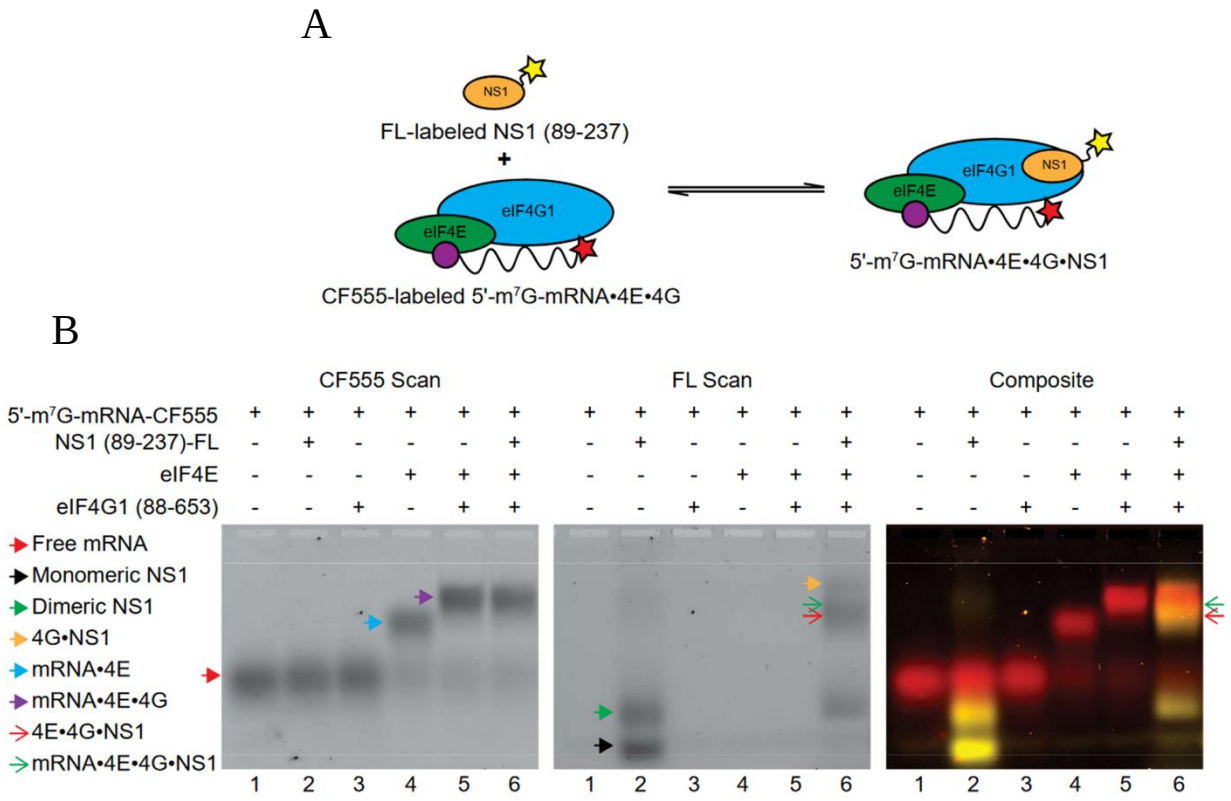

Figure 2.6.1: Electrophoretic mobility shift assay depicting the colocalization of the fluorescently labeled NS1 (89-237) with the CF555-labeled 5'-m^{7}G-mRNA bound to the eIF4E•eIF4G complex. (A) A cartoon illustrating the binding of NS1 to the eIF4E•eIF4G complex. (B) An EMSA displaying the formation of the 5'-m^{7}G-mRNA•eIF4E•eIF4G•NS1 complex through the use of two individual fluorophores. The CF555 scan visualizes 5'-m^{7}G-mRNA containing complexes while the FL scan visualizes NS1 containing complexes. The composite image was produced by the overlaying if the CF555 scan (Red) and the fluorescein scan (Yellow). The plus and minus signs indicate the addition of the corresponding biomolecules. The colored arrows label the appropriate complex or fluorophore-labeled protein or mRNA. The concentrations were as followed: NS1 was 75 nM, 5'-m^{7}G-mRNA was 50 nM, eIF4E was 500 nM and eIF4G was 500 nM.

Following our success showing the formation of the 5'-m^{7}G-mRNA•eIF4E•eIF4G1•NS1 complex, we wanted to further visualize this complex formation in the presence of the other know complexes to ensure our results are genuine. We performed another EMSA where we formed the 5'-m^{7}G-mRNA•eIF4E•eIF4G1•NS1 complex along with the 4G•NS1, mRNA•4E, mRNA•4E•4G, 4E•NS1 and 4E•4G•NS1 complexes. Interestingly, the band corresponding to the

4E•4G•NS1 complex (FL Scan, Lane 7) is identical to the band pattern found in the lane containing the 5'-m^{7}G-mRNA•eIF4E•eIF4G1 complex (FL Scan, Lane 4) while retaining the orange complexion in the composite image (Composite, Lane 4) denoting the presence of both the CF-555 labeled 5'-m^{7}G-mRNA and the fluorescein labeled NS1 (89-237) (Figure 2.6.2 A). In addition, we plotted the intensity peaks of each fluorophore for each individual lane. Our plots indicate a considerable overlap between the intensity peaks of CF-555 and fluorescein in lane 4, corresponding to the 5'-m^{7}G-mRNA•eIF4E•eIF4G1•NS1 complex (Figure 2.6.2 B). Altogether, our results indicate that NS1 (89-237) can bind the eIF4E•eIF4G1 complex both when bound to and in the absence of 5'-m^{7}G-mRNA.

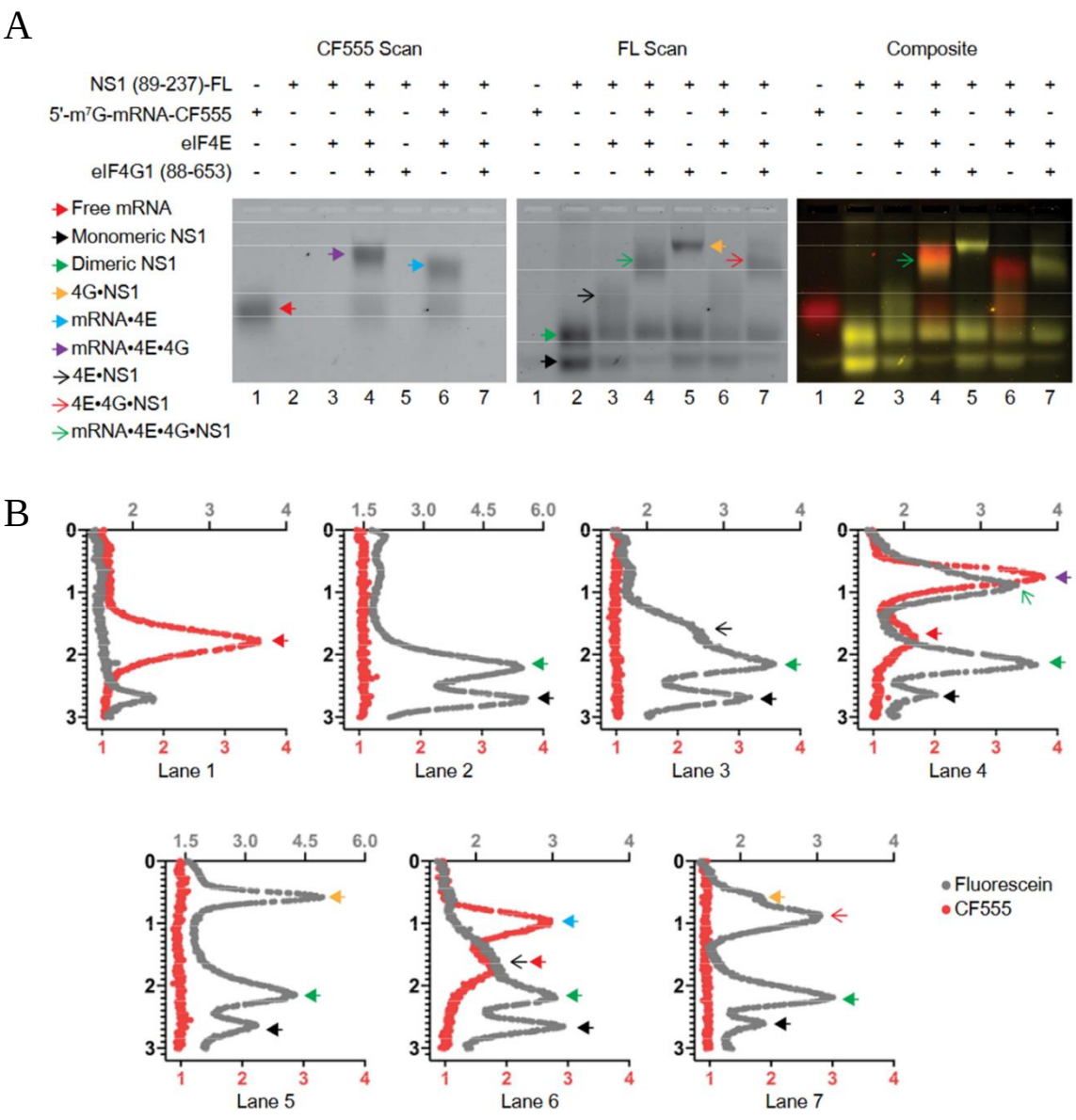

Figure 2.6.2: Band intensity analysis of the electrophoretic mobility shift assay displaying sub-complexes of the 5'-m^{7}G-mRNA•eIF4E•eIF4G•NS1 complex. (A) An EMSA displaying the formation of the 5'-m^{7}G-mRNA•eIF4E•eIF4G•NS1 complex in the context of the various NS1-containing or CF-555 containing complexes. The CF555 scan visualizes 5'-m^{7}G-mRNA containing complexes while the FL scan visualizes NS1 containing complexes. The composite image was produced by the overlaying if the CF555 scan (Red) and the fluorescein scan (Yellow). (B) Overlaid ImageJ intensity plots of the CF555 scan (Red) and the Fl scan (Grey). The top horizontal axis corresponds to the relative intensity of the FL scan while the bottom horizontal axis corresponds to the relative intensity of the CF555 scan. The vertical axis is the distance from the top to the bottom of the gel (centimeters). The plus and minus signs indicate the addition of the corresponding biomolecules. The colored arrows label the appropriate complex or fluorophore-labeled protein or mRNA. The concentrations were as followed: NS1 was 75 nM, 5'-m^{7}G-mRNA was 50 nM, eIF4E was 500 nM and eIF4G was 500 nM.

Chapter 3: Conclusion and Future Directions

Conclusion

Our EMSA experiments have shown that H3N2 NS1 (89-237) can bind the eIF4E•eIF4G1 complex, with and without mRNA, presumably through binding eIF4G1 as eIF4G1 functions as a scaffolding protein which is able to bind multiple proteins simultaneously[89,90]. In addition to binding the eIF4E•eIF4G1 complex, our data also showed NS1's ability to bind eIF4E but only in the absence of 5'-m^{7}G-mRNA. Though uncertain, we reason NS1 may target eIF4E in an antagonistic manner, although more experiments need to be performed.

Though the reason as to why NS1 may bind the eIF4E•eIF4G1 complex is still unclear, we speculate it may help explain how NS1 stimulates cap-dependent translation as shown previously [33,78,91,92]. As such we theorize NS1 may help facilitate the formation of the mRNA•eIF4E•eIF4G1 complex and the 40S containing pre-initiation complex through their respective interactions with NS1 leading to cap-dependent translation stimulation (Figure 3).

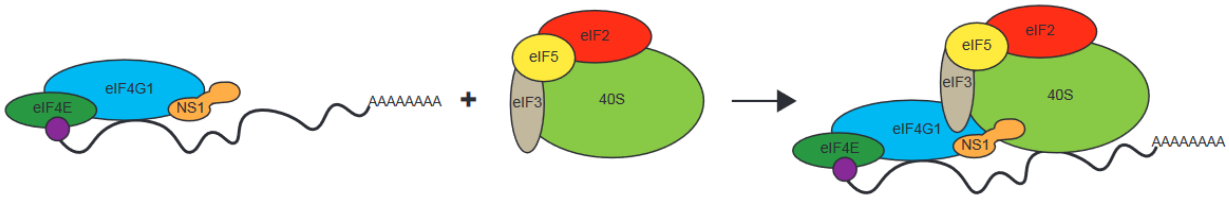

Figure 3: Model for NS1's stimulation of cap-dependent translation. NS1 may use a network of interactions to unite the 5'-m^{7}G-mRNA bound eIF4E•eIF4G complex and the 40S containing pre-initiation complex together to stimulate cap-dependent translation.

3.1 The interaction of NS1 and PABP in the context of the eIF4E•eIF4G1 complex

Following our initial results, we noted only the C-terminal amino acids (89-237) are needed for the interaction with the eIF4E•eIF4G1 complex, implying the N-terminal end of NS1 is unbound or unoccupied. Interestingly, previous studies have demonstrated that only the N-terminal end of the NS1 protein is needed to bind PABP1, a protein necessary for the formation of the closed-loop structure when translating mRNA[46–48]. In conjunction, a previous study found NS1 associated with PABP1 and eIF4G1 in viral mRNA translation initiation complexes[47]. Together, these results allude to an interesting NS1 hypothesis. Could NS1 act as an intermediate that stimulates translation by assisting the binding of PABP1 to the eIF4F complex through the interactions of both the N-terminal end (PABP1 binding site) and C-terminal end (mRNA•eIF4E•eIF4G1 binding site)? As such, the next logical step would be to include PABP in the EMSA experiments to see if there is a distinct difference between PABP binding to eIF4G1 in the presence of NS1 (89-237) versus in the presence of full-length NS1.

3.2 Amino Acid mapping of the NS1 and eIF4E interaction

Our results have introduced a previously unknown NS1 interaction with the human eIF4E cap-binding protein. Since our studies used a C-terminal NS1 mutant protein (amino acids 89 through 237) and the full-length eIF4E protein, there are still unanswered questions regarding where the binding sites are located on the proteins. Mapping the amino acids corresponding to the NS1 binding site on eIF4E will serve to better understand why NS1 is unable to bind the mRNA•eIF4E complex. Additionally, mapping the amino acids corresponding to the eIF4E binding site on NS1 will allow us to determine whether there is any overlap between the eIF4E

binding site on NS1 and the eIF4G1 binding site on NS1, which will give insight as to how NS1 binds the eIF4G1•eIF4E complex.

3.3 Solving the NS1•eIF4E structure

The protein structure of the effector domain of NS1 has been solved through both x-ray diffraction and NMR solution.[34,93] Furthermore, the protein structure of human eIF4E has also been solved using x-ray diffraction.[94] A potential experimental inquiry we have considered would look into solving the NS1•eIF4E structure either through x-ray crystallography, as both proteins form viable crystals, or through cryogenic electron microscopy if crystal formation proves too difficult.

Chapter 4: Materials and Methods

4.1 Expression, purification, and fluorescent labeling of the truncated NS1 variant

The sequence coding for wildtype Influenza A/Udorn/1972 (H3N2) spanning residues D2 to D237 was subcloned using ligation independent cloning into the expression vector pETHSUL, a plasmid containing a N-terminal hexahistidine protein tag followed by a SUMO protein tag. Amino acids D2 to R88 were deleted by PCR deletion mutagenesis in order to remove both the RNA-binding domain and the linker region of the NS1 protein, creating the NS1 (89-237) construct. Following the deletion of these regions of the protein, the sequence coding for the SUMO tag was also removed, leaving only the N-terminal hexahistidine protein tag.

The NS1 (89-237) containing pETHSUL expression plasmid was transformed in *E. coli* BL21(DE3) cells (Novagen). The *E. coli* cells were grown in a 10 mL LB starter culture supplied with 100 ug/mL ampicillin overnight. Following overnight incubation, 1 liter of LB media containing 100 ug/mL ampicillin was inoculated with 4-5 mL of the incubated cells and allowed to grow at 37°C until the OD_{600} reached a value between 0.6 and 0.8. The cultures were then induced with 1 mM IPTG and allowed to incubate for another two and a half hours at 37°C. The *E.Coli* cells were then pelleted at 5000 RPM for 15 minutes in the Beckman JLA-10.500 rotor at 4°C.

The NS1 (89-237) expressing *E.Coli* cells were re-suspended in lysis buffer containing 50 mM HEPES (pH 7.5), 300 mM NaCl, 0.5 mM EDTA, 15 mM imidazole, 5% glycerol, .1% Triton-X 100, 8 mM DTT and 1 mM PMSF. The cells were lysed by sonication, 10 cycles of an 8 second pulse and a 60 second rest. This sonication cycle was repeated once more for a total of 20 cycles. The lysate was then clarified by centrifugation at 50,000 g for 45 minutes at 4°C and

the supernatant was incubated for 1 hour with pre-equilibrated Ni-NTA beads from Qiagen. The supernatant/Ni-NTA bead mixture was loaded onto a column and the beads were washed with 10 column volumes of buffer containing 50 mM HEPES (pH 7.5), 300 mM NaCl, 0.5 mM EDTA, 40 mM imidazole, 5% glycerol, 8 mM DTT and 1 mg/mL of heparin sodium salt. Following this, the beads were rinsed with 10 column volumes of high salt buffer containing 50 mM HEPES (pH 7.5), 1 M NaCl, 0.5 mM EDTA, 40 mM imidazole, 5% glycerol and 8 mM DTT. Lastly, the beads were washed 10 column volumes of buffer containing 50 mM HEPES (pH 7.5), 300 mM NaCl, 0.5 mM EDTA, 5% glycerol and 8 mM DTT. The hexahistidine tagged NS1 (89-237) was eluted in 1 mL fractions by the addition of 12 column volumes of elution buffer containing 50 mM HEPES (pH 7.5), 300 mM NaCl, 0.5 mM EDTA, 5% glycerol, 8 mM DTT and 250 mM imidazole. The protein containing elution fractions were identified using SDS-PAGE. The fractions containing the NS1 (89-237) protein were pooled together and concentrated down to 3 mL using a Amicon Ultra Centrifugal filter. The protein sample was then loaded into a Superdex 75 16/600 gel filtration column (GE Healthcare) with buffer containing 50 mM HEPES (pH 7.5), 300 mM NaCl, 10% glycerol and .2 mM TCEP. The protein containing elution fractions were identified using SDS-PAGE. The sample was then concentrated using a Amicon Ultra Centrifugal filter and stored at -80 °C.

The effector domain variant of NS1 was fluorescently labeled at the single cystine at amino acid position 116. This was done by introducing 15-fold molar concentration of TCEP in relation to molar concentration of the protein. In addition to excess TCEP, a 10-fold excess of Fluorescein-5-Maleimide was also required to properly label the thiol group. The tube containing the protein sample was saturated with and placed under constant nitrogen gas as to avoid oxidation by the ambient oxygen gas in the laboratory air. The TCEP and Fluorescein-5-

Maleimide were injected directly to the protein sample, which was then wrapped tightly with both Parafilm and aluminum foil as to avoid oxidation and fluorescence quenching. The reaction tube was allowed to tumble at 4°C overnight to ensure the protein was successfully labeled. Following the overnight tumbling, the reaction was supplemented with 8 mM DTT in order to quench the reaction. The reaction tube was then spun for 10 minutes at 16.1 RCF in order to pellet any precipitated protein caused by the labeling reaction. To remove the free and unreacted dye, the protein sample was loaded onto a Bio-Spin 6 column (Bio-Rad) preequilibrated with buffer containing 50 mM HEPES (pH 7.5), 300 mM NaCl, 10% glycerol and .2 mM TCEP. The column was then centrifuged according to the manufacturer's instructions, this was repeated a total of three times to ensure there was minimal free-dye present in the protein sample. The diluted fluorescein-labeled protein was first filtered by a Spin-X centrifuge tube then concentrated using a Amicon Ultra Centrifugal filter and stored at -80 °C.

4.2 Expression and purification of the human eIF4G1 variant

A truncated section (amino acids 88 through 653) of the sequence coding for human eIF4G1 isoform 5 was purchased and codon optimized for expression in a *E.coli* system by GENEWIZ. This sequence was subcloned into the pTXB1 vector, a vector containing a C-terminal Mxe GyrA intein and a chitin binding domain. In order to enhance the cleavage of the Mxe GyrA intein, a threonine was inserted after amino acid D653.

The eIF4G (88-653) encoding plasmid was transformed into in *E. coli* BL21(DE3) Star cells (Novagen). The *E. coli* cells were grown in a 10 mL LB starter culture supplied with 100 ug/mL ampicillin overnight. Following overnight incubation, 1 liter of LB media containing 100

ug/mL ampicillin was inoculated with 4-5 mL of the incubated cells and allowed to grow at 37°C until the OD_{600} reached a value between 0.6 and 0.8. The culture was then cooled to 30°C and allowed to induce with 0.4 mM IPTG for two hours and a half at 30°C. The *E.Coli* cells were then pelleted at 5000 RPM for 15 minutes in the Beckman JLA-10.500 rotor at 4°C.

The cells containing eIF4G (88-653) were resuspended in buffer containing 20 mM HEPES (pH 8.2), 1 M KCl, 20% glycerol, 1 mM EDTA, 1 mM PMSF. The cells were lysed by sonication, subjecting the cells to 10 cycles of an 8 second pulse and a 60 second rest. This sonication cycle was repeated once more for a total of 20 cycles. The lysate was then clarified by centrifugation at 50,000 g for 45 minutes at 4°C and supernatant was incubated at 4°C for two and a half hours with pre-equilibrated chitin resin from NEB. Following the incubation period, the beads were loaded onto a column and allowed the liquid to flow through the beads. Following this, the beads were washed with 8 column volumes of buffer containing 20 mM HEPES (pH 7.5), 100 mM KCl, 10% glycerol, 0.1 mM EDTA, 0.5 mM TCEP and 1 mg/mL of heparin sodium salt. Then the beads were washed with 24 column volumes of buffer containing 20 mM HEPES (pH 8.2), 1 M KCl, 20% glycerol, 1 mM EDTA. The beads were then rinsed with 8 column volumes of buffer containing 20 mM HEPES (pH 7.5), 100 mM KCl, 10% glycerol, 0.1 mM EDTA, 0.5 mM TCEP. Following the draining of the previous wash buffer, 4 column volumes of a buffer containing 20 mM HEPES (pH 7.5), 100 mM KCl, 10% glycerol, 0.1 mM EDTA, 0.5 mM TCEP and 50 mM DTT was added to the beads in order to catalyze the cleaving reaction of the Mxe GyrA intein found on the C-terminal of eIF4G (88-653). The beads in solution were allowed to tumble overnight at room temperature to maximize the amount of cleaved protein. Following the cleavage reaction, the solution was drained from the beads and concentrated to 4 mL by an Amicon Ultra Centrifugal filter then loaded into a Superdex 75

16/600 gel filtration column (GE Healthcare) with buffer containing 20 mM HEPES (pH 7.5), 100 mM KCl, 10% glycerol, 0.1 mM EDTA, 0.5 mM TCEP. The protein containing elution fractions were identified using SDS-PAGE. The fractions containing the eIF4G variant were pooled together and concentrated using a Amicon Ultra Centrifugal filter then filtered using a Spin-X centrifuge tube to remove any precipitated protein and stored at -80 °C.

4.3 Expression and purification of the human eIF4E

A plasmid containing the coding sequence for human eIF4E isoform 1 was purchased from Addgene and subcloned into the expression vector pMCSG26, a plasmid containing a C-terminal hexahistidine protein tag. The eIF4E encoding plasmid was then transformed into the *E. coli* expression strain Rosetta 2 (DE3) pLysS from Novagen. The cells were grown overnight in a 10 mL LB starter culture supplied with 100 ug/mL ampicillin and 25 ug/mL chloramphenicol. Following overnight incubation, 1 liter of LB media containing 100 ug/mL ampicillin and 25 ug/mL chloramphenicol was inoculated with 4-5 mL of the incubated cells and allowed to grow at 37°C until the OD_{600} reached a value of around 0.5. The culture was then cooled to 14°C and allowed to induce with 0.2 mM IPTG for 14 to 16 hours at 14°C. The cells were then centrifugated at 5000 RPM for 15 minutes to pellet at 4°C.

Cells expressing eIF4E were resuspended in a buffer containing 100 mM Tris-HCl (pH 8.0), 100 mM KCl, 10% glycerol, 5 mM imidazole, 5 mM β-mercaptoethanol and 1 mM PMSF. The cells were lysed by French press, then clarified by centrifugation at 50,000g for 45 minutes at 4°C. The clarified solution was then allowed to incubate for two hours at 4°C with preequilibrated Ni-NTA resin from Qiagen. Following the incubation period, the beads were

loaded onto a column and allowed to have the solution flow through. The beads were washed with 50 column volumes of buffer containing 100 mM Tris-HCl (pH 8.0), 100 mM KCl, 10% glycerol, 5 mM imidazole, 5 mM β-mercaptoethanol and 1 mg/mL heparin sodium salt. Then a wash of 50 column volumes with buffer containing 100 mM Tris-HCl (pH 8.0), 1 M KCl, 10% glycerol, 5 mM β-mercaptoethanol. Followed by 50 column volumes of wash buffer containing 100 mM Tris-HCl (pH 8.0), 100 mM KCl, 10% glycerol and 20 mM imidazole. The protein was eluted by adding 25 column volumes of buffer containing 20 mM Tris-HCl (pH 8.0), 100 mM KCl, 10% glycerol, 5 mM β-mercaptoethanol and 250 mM imidazole. The beads were incubated at room temperature for 15 minutes in the elution buffer, then the elutions were collected and pooled together in order to concentrate the volume to less than 5 mL. The protein sample was purified further by use of a Superdex 75 16/60 gel filtration column (GE Healthcare) with a buffer containing 20 mM Tris-HCl (pH 8.0), 100 mM NaCl and 10% glycerol. The fractions were analyzed with SDS-PAGE and the protein-containing samples were pooled together and concentrated to a volume less than 5 mL. The concentrated protein sample was then further purified by HiTrap Q anion exchange chromatography from Cytiva. One buffer containing 20 mM Tris-HCl (pH 8.0), 10% glycerol and 100 mM NaCl and another buffer containing 20 mM Tris-HCl (pH 8.0), 10% glycerol and 1 M NaCl were utilized to establish a low to high NaCl gradient to elude the eIF4E protein. The fractions were analyzed by SDS-PAGE, the fractions with the protein of interest were pooled together, concentrated using a Amicon Ultra Centrifugal filter then filtered using a Spin-X centrifuge tube to remove any precipitated protein and stored at -80 °C.

4.4 Labeled 5'-m^7G-mRNA for Electrophoretic Mobility Shift Assay

The mRNA (5′-GGGUGACAGUCCUGUUU-3′) was synthesized by T7 RNA polymerase transcription in vitro and purified by denaturing urea-PAGE, chloroform extraction and ethanol precipitation. The mRNA was resuspended in water and the concentration was determined, then stored at -80°C. The 3' end of the mRNA was fluorescently labeled by first oxidizing the 3' end with a solution consisting of 100 mM sodium acetate (pH 5.2) and 100 μM potassium periodate for an hour and 30 minutes at room temperature. Following the incubation, the mRNA was purified from the solution using a Monarch RNA Clean-up Kit (New England BioLabs). The mRNA was then incubated with either Fluorescein 5-thiosemicarbizide (Invitrogen) or CF-555 hydrazide (Biotium) overnight at 4°C. The newly labeled mRNA then had a 7-methylguanylate cap was added to the 5' end of using the vaccinia capping enzyme.

4.5 Fluorescence anisotropy binding assay and equilibrium dissociation constant determination

Both the eIF4G1 (88-653) construct and wildtype human eIF4E were titrated against 20 nM of the fluorescein-labeled NS1 (89-237). Fluorescence anisotropy was measured on a non-binding 384 well, black bottom plate (Greiner) using a Spark multimode microplate reader from Tecan.

When appropriate, the proteins were diluted using buffer containing 50 mM HEPES (pH 7.4), 150 mM NaCl, 10% glycerol. Reactions were carried out in buffer containing 50 mM HEPES (pH 7.4), 150 mM NaCl, 5% glycerol and .01% Tween-20. Each reaction contained a total volume of 30 uL and was allowed to incubate in darkness, at room temperature for 1 hour

before measuring the fluorescence. Samples were excited at 485 nm with a bandwidth of 20 nm and emission was measured at 535 nm with a bandwidth of 25 nm. The optimal gain and Z-position were determined per read.

Bovine serum albumin was titrated against the fluorescein-labeled NS1 (89-237) to measure its native ability to non-specifically bind proteins under identical binding conditions.

The equilibrium dissociation constant (K_D) for NSl-ED and eIF4G1 (88-653), and the equilibrium dissociation constant for NS1 (89-237) and wildtype eIF4E were quantified by fitting the anisotropy data from each binding assay to the equation below. The fluorescein-labeled NS1 (89-237) $[L]_t$ was fixed at 20 nM while eIF4G1 (88-653) or wildtype eIF4E was varied over a range of concentrations $[R]_t$ to calculate the K_D using GraphPad Prism.

$$\frac{[P+FL]}{[FL]} = \frac{\left[[P]+[FL]+K_D-\sqrt{([P]+[FL]+K_D)^2-4[P][FL]}\right]}{(2[P])}$$

4.6 Electrophoresis mobility shift assay and intensity percentage shift

Similar to the anisotropic binding assay described above, both the eIF4G1 (88-653) construct and wildtype human eIF4E were titrated against 100 nM of the fluorescein-labeled NS1 (89-237) construct. When appropriate, the proteins were diluted using buffer containing 50 mM HEPES (pH 7.4), 150 mM NaCl, 10% glycerol. Reactions were carried out in buffer containing 50 mM HEPES (pH 7.4), 150 mM NaCl, 5% glycerol and .01% Tween-20. Each reaction contained a total volume of 20 uL and was allowed to incubate in darkness, at room temperature for 1 hour before supplementing 1.5 uL of chilled loading buffer containing 50% glycerol and xylene cyanol. The samples were loaded in a .07% SeaKem GTG agarose gel

(Lonza) containing .5X TBE buffer. The gels ran at 66 volts for 1 hour and 15 minutes at 4°C and were visualized using a Typhoon FLA9500 from GE Life Science.

Bovine serum albumin was substituted in place of eIF4G (88-653) and eIF4E in order to measure any non-specific binding of the fluorescein-labeled NS1 (89-237) under identical binding conditions.

The visualized gels were quantified using the image analyzing software ImageJ from the National Institutes of Health. Each band had its corresponding mean intensity measured along with the area the band encompassed, this was repeated for the total intensity of the lane and total area of the lane. The mean intensity was then multiplied by its area, producing an intensity value of the given area. This value was then divided by the intensity value of the entire lane. This calculated value was defined as the relative intensity percentage of the lane. This was done for each lane, allowing for a relative intensity percentage shift to be quantified as the titrated protein concentration increased.

References

(1) Peteranderl, C.; Herold, S.; Schmoldt, C. Human Influenza Virus Infections. *Semin. Respir. Crit. Care Med.* **2016**, *37* (4), 487–500. https://doi.org/10.1055/s-0036-1584801.

(2) Mostafa, A.; Abdelwhab, E. M.; Mettenleiter, T. C.; Pleschka, S. Zoonotic Potential of Influenza A Viruses: A Comprehensive Overview. *Viruses* **2018**, *10* (9). https://doi.org/10.3390/v10090497.

(3) Munoz, O.; De Nardi, M.; van der Meulen, K.; van Reeth, K.; Koopmans, M.; Harris, K.; von Dobschuetz, S.; Freidl, G.; Meijer, A.; Breed, A.; Hill, A.; Kosmider, R.; Banks, J.; Stärk, K. D. C.; Wieland, B.; Stevens, K.; van der Werf, S.; Enouf, V.; Dauphin, G.; Dundon, W.; Cattoli, G.; Capua, I.; FLURISK Consortium. Genetic Adaptation of Influenza A Viruses in Domestic Animals and Their Potential Role in Interspecies Transmission: A Literature Review. *EcoHealth* **2016**, *13* (1), 171–198. https://doi.org/10.1007/s10393-014-1004-1.

(4) Taubenberger, J. K.; Morens, D. M. The 1918 Influenza Pandemic and Its Legacy. *Cold Spring Harb. Perspect. Med.* **2020**, *10* (10). https://doi.org/10.1101/cshperspect.a038695.

(5) Johnson, N. P. A. S.; Mueller, J. Updating the Accounts: Global Mortality of the 1918-1920 "Spanish" Influenza Pandemic. *Bull. Hist. Med.* **2002**, *76* (1), 105–115. https://doi.org/10.1353/bhm.2002.0022.

(6) Rolfes, M. A.; Foppa, I. M.; Garg, S.; Flannery, B.; Brammer, L.; Singleton, J. A.; Burns, E.; Jernigan, D.; Olsen, S. J.; Bresee, J.; Reed, C. Annual Estimates of the Burden of Seasonal Influenza in the United States: A Tool for Strengthening Influenza Surveillance and Preparedness. *Influenza Other Respir. Viruses* **2018**, *12* (1), 132–137. https://doi.org/10.1111/irv.12486.

(7) Reed, C.; Chaves, S. S.; Kirley, P. D.; Emerson, R.; Aragon, D.; Hancock, E. B.; Butler, L.; Baumbach, J.; Hollick, G.; Bennett, N. M.; Laidler, M. R.; Thomas, A.; Meltzer, M. I.; Finelli, L. Estimating Influenza Disease Burden from Population-Based Surveillance Data in the United States. *PLOS ONE* **2015**, *10* (3), e0118369. https://doi.org/10.1371/journal.pone.0118369.

(8) Putri, W. C. W. S.; Muscatello, D. J.; Stockwell, M. S.; Newall, A. T. Economic Burden of Seasonal Influenza in the United States. *Vaccine* **2018**, *36* (27), 3960–3966. https://doi.org/10.1016/j.vaccine.2018.05.057.

(9) Molinari, N.-A. M.; Ortega-Sanchez, I. R.; Messonnier, M. L.; Thompson, W. W.; Wortley, P. M.; Weintraub, E.; Bridges, C. B. The Annual Impact of Seasonal Influenza in the US: Measuring Disease Burden and Costs. *Vaccine* **2007**, *25* (27), 5086–5096. https://doi.org/10.1016/j.vaccine.2007.03.046.

(10) Iuliano, A. D.; Roguski, K. M.; Chang, H. H.; Muscatello, D. J.; Palekar, R.; Tempia, S.; Cohen, C.; Gran, J. M.; Schanzer, D.; Cowling, B. J.; Wu, P.; Kyncl, J.; Ang, L. W.; Park, M.;

Redlberger-Fritz, M.; Yu, H.; Espenhain, L.; Krishnan, A.; Emukule, G. Estimates of Global Seasonal Influenza-Associated Respiratory Mortality: A Modelling Study. **2019**, 31.

(11) Taubenberger, J. K.; Morens, D. M. The Pathology of Influenza Virus Infections. **2008**, 28.

(12) Uyeki, T. M.; Peiris, M. Novel Avian Influenza A Virus Infections of Humans. *Infect. Dis. Clin. North Am.* **2019**, *33* (4), 907–932. https://doi.org/10.1016/j.idc.2019.07.003.

(13) Keilman, L. J. Seasonal Influenza (Flu). *Nurs. Clin. North Am.* **2019**, *54* (2), 227–243. https://doi.org/10.1016/j.cnur.2019.02.009.

(14) Brienen, N. C. J.; Timen, A.; Wallinga, J.; Van Steenbergen, J. E.; Teunis, P. F. M. The Effect of Mask Use on the Spread of Influenza During a Pandemic. *Risk Anal.* **2010**, *30* (8), 1210–1218. https://doi.org/10.1111/j.1539-6924.2010.01428.x.

(15) Epperson, S.; Davis, C. T.; Brammer, L.; Elal, A. I. A.; Ajayi, N.; Barnes, J.; Burns, E.; Daly, P.; Dugan, V. G.; Fry, A. M.; Jang, Y.; Johnson, S. J.; Kondor, R.; Grohskopf, L. A.; Gubareva, L.; Merced-Morales, A.; Sessions, W.; Stevens, J.; Wentworth, D. E.; Xu, X.; Jernigan, D. Update: Influenza Activity — United States and Worldwide, May 19–September 28, 2019, and Composition of the 2020 Southern Hemisphere Influenza Vaccine. **2019**, *68* (40), 5.

(16) Grohskopf, L. A.; Alyanak, E.; Broder, K. R.; Walter, E. B.; Fry, A. M.; Jernigan, D. B. Prevention and Control of Seasonal Influenza with Vaccines: Recommendations of the Advisory Committee on Immunization Practices — United States, 2019–20 Influenza Season. *MMWR Recomm. Rep.* **2019**, *68* (3), 1–21. https://doi.org/10.15585/mmwr.rr6803a1.

(17) Lambert, L. C.; Fauci, A. S. Influenza Vaccines for the Future. *N. Engl. J. Med.* **2010**, *363* (21), 2036–2044. https://doi.org/10.1056/NEJMra1002842.

(18) Hutchinson, E. C. Influenza Virus. *Trends Microbiol.* **2018**, *26* (9), 809–810. https://doi.org/10.1016/j.tim.2018.05.013.

(19) Bouvier, N. M.; Palese, P. THE BIOLOGY OF INFLUENZA VIRUSES. *Vaccine* **2008**, *26* (Suppl 4), D49–D53.

(20) Webster, R. G.; Bean, W. J.; Gorman, O. T.; Chambers, T. M.; Kawaoka, Y. Evolution and Ecology of Influenza A Viruses. *Microbiol. Mol. Biol. Rev.* **1992**, *56* (1), 152–179.

(21) Paterson, D.; Fodor, E. Emerging Roles for the Influenza A Virus Nuclear Export Protein (NEP). *PLoS Pathog.* **2012**, *8* (12), e1003019. https://doi.org/10.1371/journal.ppat.1003019.

(22) Inglis, S. C.; Barrett, T.; Brown, C. M.; Almond, J. W. The Smallest Genome RNA Segment of Influenza Virus Contains Two Genes That May Overlap. *Proc. Natl. Acad. Sci. U. S. A.* **1979**, *76* (8), 3790–3794.

(23) Yamauchi, Y. Chapter One - Influenza A Virus Uncoating. In *Advances in Virus Research*; Kielian, M., Mettenleiter, T. C., Roossinck, M. J., Eds.; Academic Press, 2020; Vol. 106, pp 1–38. https://doi.org/10.1016/bs.aivir.2020.01.001.

(24) Du, R.; Cui, Q.; Rong, L. Competitive Cooperation of Hemagglutinin and Neuraminidase during Influenza A Virus Entry. *Viruses* **2019**, *11* (5). https://doi.org/10.3390/v11050458.

(25) Vahey, M. D.; Fletcher, D. A. Influenza A Virus Surface Proteins Are Organized to Help Penetrate Host Mucus. *eLife 8*. https://doi.org/10.7554/eLife.43764.

(26) Edinger, T. O.; Pohl, M. O.; Stertz, S. Entry of Influenza A Virus: Host Factors and Antiviral Targets. *J. Gen. Virol.* **2014**, *95* (2), 263–277. https://doi.org/10.1099/vir.0.059477-0.

(27) Poon, L. L. M.; Pritlove, D. C.; Sharps, J.; Brownlee, G. G. The RNA Polymerase of Influenza Virus, Bound to the 5′ End of Virion RNA, Acts in Cis To Polyadenylate MRNA. *J. Virol.* **1998**, *72* (10), 8214–8219.

(28) Poon, L. L.; Pritlove, D. C.; Fodor, E.; Brownlee, G. G. Direct Evidence That the Poly(A) Tail of Influenza A Virus MRNA Is Synthesized by Reiterative Copying of a U Track in the Virion RNA Template. *J. Virol.* **1999**, *73* (4), 3473–3476. https://doi.org/10.1128/JVI.73.4.3473-3476.1999.

(29) Robertson, J. S.; Schubert, M.; Lazzarini, R. A. Polyadenylation Sites for Influenza Virus MRNA. *J. Virol.* **1981**, *38* (1), 157–163.

(30) Anhäuser, L.; Hüwel, S.; Zobel, T.; Rentmeister, A. Multiple Covalent Fluorescence Labeling of Eukaryotic MRNA at the Poly(A) Tail Enhances Translation and Can Be Performed in Living Cells. *Nucleic Acids Res.* **2019**, *47* (7), e42. https://doi.org/10.1093/nar/gkz084.

(31) Rossman, J. S.; Lamb, R. A. Influenza Virus Assembly and Budding. *Virology* **2011**, *411* (2), 229–236. https://doi.org/10.1016/j.virol.2010.12.003.

(32) Pohl, M. O.; Lanz, C.; Stertz, S. Late Stages of the Influenza A Virus Replication Cycle-a Tight Interplay between Virus and Host. *J. Gen. Virol.* **2016**, *97* (9), 2058–2072. https://doi.org/10.1099/jgv.0.000562.

(33) Hale, B. G.; Randall, R. E.; Ortín, J.; Jackson, D. The Multifunctional NS1 Protein of Influenza A Viruses. *J. Gen. Virol.* **2008**, *89* (10), 2359–2376. https://doi.org/10.1099/vir.0.2008/004606-0.

(34) Bornholdt, Z. A.; Prasad, B. V. V. X-Ray Structure of NS1 from a Highly Pathogenic H5N1 Influenza Virus. *Nature* **2008**, *456* (7224), 985–988. https://doi.org/10.1038/nature07444.

(35) Jureka, A. S.; Kleinpeter, A. B.; Cornilescu, G.; Cornilescu, C. C.; Petit, C. M. Structural Basis for a Novel Interaction between the NS1 Protein Derived from the 1918 Influenza Virus and RIG-I. *Struct. Lond. Engl. 1993* **2015**, *23* (11), 2001–2010. https://doi.org/10.1016/j.str.2015.08.007.

(36) Kleinpeter, A. B.; Jureka, A. S.; Falahat, S. M.; Green, T. J.; Petit, C. M. Structural Analyses Reveal the Mechanism of Inhibition of Influenza Virus NS1 by Two Antiviral Compounds. *J. Biol. Chem.* **2018**, *293* (38), 14659–14668. https://doi.org/10.1074/jbc.RA118.004012.

(37) Carrillo, B.; Choi, J.-M.; Bornholdt, Z. A.; Sankaran, B.; Rice, A. P.; Prasad, B. V. V. The Influenza A Virus Protein NS1 Displays Structural Polymorphism. *J. Virol.* **2014**, *88* (8), 4113–4122. https://doi.org/10.1128/JVI.03692-13.

(38) Li, W.; Noah, J. W.; Noah, D. L. Alanine Substitutions within a Linker Region of the Influenza A Virus Non-Structural Protein 1 Alter Its Subcellular Localization and Attenuate Virus Replication. *J. Gen. Virol.* **2011**, *92* (Pt 8), 1832–1842. https://doi.org/10.1099/vir.0.031336-0.

(39) Han, C. W.; Jang, M. S. J. and S. B. Structure and Function of the Influenza A Virus Non-Structural Protein 1. **2019**, *29* (8), 1184–1192. https://doi.org/10.4014/jmb.1903.03053.

(40) Mitra, S.; Kumar, D.; Hu, L.; Sankaran, B.; Moosa, M. M.; Rice, A. P.; Ferreon, J. C.; Ferreon, A. C. M.; Prasad, B. V. V. Influenza A Virus Protein NS1 Exhibits Strain-Independent Conformational Plasticity. *J. Virol.* **2019**, *93* (21). https://doi.org/10.1128/JVI.00917-19.

(41) Shim, J. M.; Kim, J.; Tenson, T.; Min, J.-Y.; Kainov, D. E. Influenza Virus Infection, Interferon Response, Viral Counter-Response, and Apoptosis. *Viruses* **2017**, *9* (8). https://doi.org/10.3390/v9080223.

(42) García-Sastre, A.; Egorov, A.; Matassov, D.; Brandt, S.; Levy, D. E.; Durbin, J. E.; Palese, P.; Muster, T. Influenza A Virus Lacking the NS1 Gene Replicates in Interferon-Deficient Systems. *Virology* **1998**, *252* (2), 324–330. https://doi.org/10.1006/viro.1998.9508.

(43) Twu, K. Y.; Noah, D. L.; Rao, P.; Kuo, R.-L.; Krug, R. M. The CPSF30 Binding Site on the NS1A Protein of Influenza A Virus Is a Potential Antiviral Target. *J. Virol.* **2006**, *80* (8), 3957–3965. https://doi.org/10.1128/JVI.80.8.3957-3965.2006.

(44) Nemeroff, M. E.; Barabino, S. M.; Li, Y.; Keller, W.; Krug, R. M. Influenza Virus NS1 Protein Interacts with the Cellular 30 KDa Subunit of CPSF and Inhibits 3'end Formation of Cellular Pre-MRNAs. *Mol. Cell* **1998**, *1* (7), 991–1000. https://doi.org/10.1016/s1097-2765(00)80099-4.

(45) Noah, D. L.; Twu, K. Y.; Krug, R. M. Cellular Antiviral Responses against Influenza A Virus Are Countered at the Posttranscriptional Level by the Viral NS1A Protein via Its Binding to a Cellular Protein Required for the 3' End Processing of Cellular Pre-MRNAS. *Virology* **2003**, *307* (2), 386–395. https://doi.org/10.1016/s0042-6822(02)00127-7.

(46) Arias-Mireles, B. H.; de Rozieres, C. M.; Ly, K.; Joseph, S. RNA Modulates the Interaction between Influenza A Virus NS1 and Human PABP1. *Biochemistry* **2018**, *57* (26), 3590–3598. https://doi.org/10.1021/acs.biochem.8b00218.

(47) Burgui, I.; Aragón, T.; Ortín, J.; Nieto, A. PABP1 and EIF4GI Associate with Influenza Virus NS1 Protein in Viral MRNA Translation Initiation Complexes. *J. Gen. Virol.* **2003**, *84* (12), 3263–3274. https://doi.org/10.1099/vir.0.19487-0.

(48) de Rozières, C. M.; Joseph, S. Influenza A Virus NS1 Protein Binds as a Dimer to RNA-Free PABP1 but Not to the PABP1·Poly(A) RNA Complex. *Biochemistry* **2020**, *59* (46), 4439–4448. https://doi.org/10.1021/acs.biochem.0c00666.

(49) Chen, Z.; Li, Y.; Krug, R. M. Influenza A Virus NS1 Protein Targets Poly(A)-Binding Protein II of the Cellular 3'-End Processing Machinery. *EMBO J.* **1999**, *18* (8), 2273–2283. https://doi.org/10.1093/emboj/18.8.2273.

(50) Koliopoulos, M. G.; Lethier, M.; van der Veen, A. G.; Haubrich, K.; Hennig, J.; Kowalinski, E.; Stevens, R. V.; Martin, S. R.; Reis e Sousa, C.; Cusack, S.; Rittinger, K. Molecular Mechanism of Influenza A NS1-Mediated TRIM25 Recognition and Inhibition. *Nat. Commun.* **2018**, *9* (1), 1820. https://doi.org/10.1038/s41467-018-04214-8.

(51) Gack, M. U.; Albrecht, R. A.; Urano, T.; Inn, K.-S.; Huang, I.-C.; Carnero, E.; Farzan, M.; Inoue, S.; Jung, J. U.; García-Sastre, A. Influenza A Virus NS1 Targets the Ubiquitin Ligase TRIM25 to Evade Recognition by the Host Viral RNA Sensor RIG-I. *Cell Host Microbe* **2009**, *5* (5), 439–449. https://doi.org/10.1016/j.chom.2009.04.006.

(52) Cheong, W.-C.; Kang, H.-R.; Yoon, H.; Kang, S.-J.; Ting, J. P.-Y.; Song, M. J. Influenza A Virus NS1 Protein Inhibits the NLRP3 Inflammasome. *PLoS ONE* **2015**, *10* (5). https://doi.org/10.1371/journal.pone.0126456.

(53) Zhang, K.; Xie, Y.; Muñoz-Moreno, R.; Wang, J.; Zhang, L.; Esparza, M.; García-Sastre, A.; Fontoura, B. M. A.; Ren, Y. Structural Basis for Influenza Virus NS1 Protein Block of MRNA Nuclear Export. *Nat. Microbiol.* **2019**, *4* (10), 1671–1679. https://doi.org/10.1038/s41564-019-0482-x.

(54) Ampomah, P. B.; Lim, L. H. K. Influenza A Virus-Induced Apoptosis and Virus Propagation. *Apoptosis Int. J. Program. Cell Death* **2020**, *25* (1–2), 1–11. https://doi.org/10.1007/s10495-019-01575-3.

(55) Li, Y.; Anderson, D. H.; Liu, Q.; Zhou, Y. Mechanism of Influenza A Virus NS1 Protein Interaction with the P85beta, but Not the P85alpha, Subunit of Phosphatidylinositol 3-Kinase (PI3K) and up-Regulation of PI3K Activity. *J. Biol. Chem.* **2008**, *283* (34), 23397–23409. https://doi.org/10.1074/jbc.M802737200.

(56) Tan, S. L.; Katze, M. G. Biochemical and Genetic Evidence for Complex Formation between the Influenza A Virus NS1 Protein and the Interferon-Induced PKR Protein Kinase. *J. Interferon Cytokine Res. Off. J. Int. Soc. Interferon Cytokine Res.* **1998**, *18* (9), 757–766. https://doi.org/10.1089/jir.1998.18.757.

(57) Hale, B. G.; Batty, I. H.; Downes, C. P.; Randall, R. E. Binding of Influenza A Virus NS1 Protein to the Inter-SH2 Domain of P85 Suggests a Novel Mechanism for Phosphoinositide 3-Kinase Activation. *J. Biol. Chem.* **2008**, *283* (3), 1372–1380. https://doi.org/10.1074/jbc.M708862200.

(58) Shin, Y.-K.; Li, Y.; Liu, Q.; Anderson, D. H.; Babiuk, L. A.; Zhou, Y. SH3 Binding Motif 1 in Influenza A Virus NS1 Protein Is Essential for PI3K/Akt Signaling Pathway Activation. *J. Virol.* **2007**, *81* (23), 12730–12739. https://doi.org/10.1128/JVI.01427-07.

(59) Bg, H.; D, J.; Yh, C.; Ra, L.; Re, R. Influenza A virus NS1 protein binds p85beta and activates phosphatidylinositol-3-kinase signaling https://pubmed.ncbi.nlm.nih.gov/16963558/ (accessed 2020 -12 -29). https://doi.org/10.1073/pnas.0606109103.

(60) Li, W.; Wang, G.; Zhang, H.; Xin, G.; Zhang, D.; Zeng, J.; Chen, X.; Xu, Y.; Cui, Y.; Li, K. Effects of NS1 Variants of H5N1 Influenza Virus on Interferon Induction, TNFα Response and P53 Activity. *Cell. Mol. Immunol.* **2010**, *7* (3), 235–242. https://doi.org/10.1038/cmi.2010.6.

(61) Wang, X.; Shen, Y.; Qiu, Y.; Shi, Z.; Shao, D.; Chen, P.; Tong, G.; Ma, Z. The Non-Structural (NS1) Protein of Influenza A Virus Associates with P53 and Inhibits P53-Mediated Transcriptional Activity and Apoptosis. *Biochem. Biophys. Res. Commun.* **2010**, *395* (1), 141–145. https://doi.org/10.1016/j.bbrc.2010.03.160.

(62) Terrier, O.; Diederichs, A.; Dubois, J.; Cartet, G.; Lina, B.; Bourdon, J.-C.; Rosa-Calatrava, M. Influenza NS1 Interacts with P53 and Alters Its Binding to P53-Responsive Genes, in a Promoter-Dependent Manner. *FEBS Lett.* **2013**, *587* (18), 2965–2971. https://doi.org/10.1016/j.febslet.2013.08.006.

(63) Pizzorno, A.; Dubois, J.; Machado, D.; Cartet, G.; Traversier, A.; Julien, T.; Lina, B.; Bourdon, J.-C.; Rosa-Calatrava, M.; Terrier, O. Influenza A Viruses Alter the Stability and Antiviral Contribution of Host E3-Ubiquitin Ligase Mdm2 during the Time-Course of Infection. *Sci. Rep.* **2018**, *8* (1), 3746. https://doi.org/10.1038/s41598-018-22139-6.

(64) Hatada, E.; Saito, S.; Okishio, N.; Fukuda, R. Binding of the Influenza Virus NS1 Protein to Model Genome RNAs. *J. Gen. Virol.* **1997**, *78* (5), 1059–1063. https://doi.org/10.1099/0022-1317-78-5-1059.

(65) Hatada, E.; Fukuda, R. Binding of Influenza A Virus NS1 Protein to DsRNA in Vitro. *J. Gen. Virol.* **1992**, *73* (12), 3325–3329. https://doi.org/10.1099/0022-1317-73-12-3325.

(66) Cheng, A.; Wong, S. M.; Yuan, Y. A. Structural Basis for DsRNA Recognition by NS1 Protein of Influenza A Virus. *Cell Res.* **2009**, *19* (2), 187–195. https://doi.org/10.1038/cr.2008.288.

(67) Talon, J.; Horvath, C. M.; Polley, R.; Basler, C. F.; Muster, T.; Palese, P.; García-Sastre, A. Activation of Interferon Regulatory Factor 3 Is Inhibited by the Influenza A Virus NS1 Protein. *J. Virol.* **2000**, *74* (17), 7989–7996. https://doi.org/10.1128/jvi.74.17.7989-7996.2000.

(68) Marión, R. M.; Zürcher, T.; de la Luna, S.; Ortín, J. Influenza Virus NS1 Protein Interacts with Viral Transcription-Replication Complexes in Vivo. *J. Gen. Virol.* **1997**, *78 (Pt 10)*, 2447–2451. https://doi.org/10.1099/0022-1317-78-10-2447.

(69) Qiu, Y.; Krug, R. M. The Influenza Virus NS1 Protein Is a Poly(A)-Binding Protein That Inhibits Nuclear Export of MRNAs Containing Poly(A). *J. Virol.* **1994**, *68* (4), 2425–2432.

(70) Inglis, S. C. Inhibition of Host Protein Synthesis and Degradation of Cellular MRNAs During Infection by Influenza and Herpes Simplex Virus. *Mol. Cell. Biol.* **1982**, *2* (12), 1644–1648.

(71) de la Luna, S.; Fortes, P.; Beloso, A.; Ortín, J. Influenza Virus NS1 Protein Enhances the Rate of Translation Initiation of Viral MRNAs. *J. Virol.* **1995**, *69* (4), 2427–2433.

(72) Enami, K.; Sato, T. A.; Nakada, S.; Enami, M. Influenza Virus NS1 Protein Stimulates Translation of the M1 Protein. *J. Virol.* **1994**, *68* (3), 1432–1437.

(73) Park, Y. W.; Katze, M. G. Translational Control by Influenza Virus. Identification of Cis-Acting Sequences and Trans-Acting Factors Which May Regulate Selective Viral MRNA Translation. *J. Biol. Chem.* **1995**, *270* (47), 28433–28439. https://doi.org/10.1074/jbc.270.47.28433.

(74) Ortín, J. Multiple Levels of Posttranscriptional Regulation of Influenza Virus Gene Expression. *Semin. Virol.* **1998**, *8* (4), 335–342. https://doi.org/10.1006/smvy.1997.0136.

(75) Garfinkel, M. S.; Katze, M. G. Translational Control by Influenza Virus. Selective Translation Is Mediated by Sequences within the Viral MRNA 5'-Untranslated Region. *J. Biol. Chem.* **1993**, *268* (30), 22223–22226.

(76) Marión, R. M.; Aragón, T.; Beloso, A.; Nieto, A.; Ortín, J. The N-Terminal Half of the Influenza Virus NS1 Protein Is Sufficient for Nuclear Retention of MRNA and Enhancement of Viral MRNA Translation. *Nucleic Acids Res.* **1997**, *25* (21), 4271–4277. https://doi.org/10.1093/nar/25.21.4271.

(77) Salvatore, M.; Basler, C. F.; Parisien, J.-P.; Horvath, C. M.; Bourmakina, S.; Zheng, H.; Muster, T.; Palese, P.; García-Sastre, A. Effects of Influenza A Virus NS1 Protein on Protein Expression: The NS1 Protein Enhances Translation and Is Not Required for Shutoff of Host Protein Synthesis. *J. Virol.* **2002**, *76* (3), 1206–1212. https://doi.org/10.1128/jvi.76.3.1206-1212.2002.

(78) Panthu, B.; Terrier, O.; Carron, C.; Traversier, A.; Corbin, A.; Balvay, L.; Lina, B.; Rosa-Calatrava, M.; Ohlmann, T. The NS1 Protein from Influenza Virus Stimulates Translation Initiation by Enhancing Ribosome Recruitment to MRNAs. *J. Mol. Biol.* **2017**, *429* (21), 3334–3352. https://doi.org/10.1016/j.jmb.2017.04.007.

(79) Katze, M. G.; Tomita, J.; Black, T.; Krug, R. M.; Safer, B.; Hovanessian, A. Influenza Virus Regulates Protein Synthesis during Infection by Repressing Autophosphorylation and Activity of the Cellular 68,000-Mr Protein Kinase. *J. Virol.* **1988**, *62* (10), 3710–3717.

(80) Katze, M. G.; Detjen, B. M.; Safer, B.; Krug, R. M. Translational Control by Influenza Virus: Suppression of the Kinase That Phosphorylates the Alpha Subunit of Initiation Factor EIF-2 and Selective Translation of Influenza Viral MRNAs. *Mol. Cell. Biol.* **1986**, *6* (5), 1741–1750.

(81) Feigenblum, D.; Schneider, R. J. Modification of Eukaryotic Initiation Factor 4F during Infection by Influenza Virus. *J. Virol.* **1993**, *67* (6), 3027–3035.

(82) Burgui, I.; Yángüez, E.; Sonenberg, N.; Nieto, A. Influenza Virus MRNA Translation Revisited: Is the EIF4E Cap-Binding Factor Required for Viral MRNA Translation? *J. Virol.* **2007**, *81* (22), 12427–12438. https://doi.org/10.1128/JVI.01105-07.

(83) Aragón, T.; Luna, S. de la; Novoa, I.; Carrasco, L.; Ortín, J.; Nieto, A. Eukaryotic Translation Initiation Factor 4GI Is a Cellular Target for NS1 Protein, a Translational Activator of Influenza Virus. *Mol. Cell. Biol.* **2000**, *20* (17), 6259–6268. https://doi.org/10.1128/MCB.20.17.6259-6268.2000.

(84) Prévôt, D.; Darlix, J.-L.; Ohlmann, T. Conducting the Initiation of Protein Synthesis: The Role of EIF4G. *Biol. Cell* **2003**, *95* (3–4), 141–156. https://doi.org/10.1016/S0248-4900(03)00031-5.

(85) Yángüez, E.; Castello, A.; Welnowska, E.; Carrasco, L.; Goodfellow, I.; Nieto, A. Functional Impairment of EIF4A and EIF4G Factors Correlates with Inhibition of Influenza Virus MRNA Translation. *Virology* **2011**, *413* (1), 93–102. https://doi.org/10.1016/j.virol.2011.02.012.

(86) Gingras, A.-C.; Raught, B.; Sonenberg, N. EIF4 Initiation Factors: Effectors of MRNA Recruitment to Ribosomes and Regulators of Translation. *Annu. Rev. Biochem.* **1999**, *68* (1), 913–963. https://doi.org/10.1146/annurev.biochem.68.1.913.

(87) Wojtczak, A.; Kasprzyk, R.; Warmiński, M.; Ubych, K.; Kubacka, D.; Sikorski, P. J.; Jemielity, J.; Kowalska, J. Evaluation of Carboxyfluorescein-Labeled 7-Methylguanine Nucleotides as Probes for Studying Cap-Binding Proteins by Fluorescence Anisotropy. *Sci. Rep.* **2021**, *11* (1), 7687. https://doi.org/10.1038/s41598-021-87306-8.

(88) Friedland, D. E.; Wooten, W. N. B.; LaVoy, J. E.; Hagedorn, C. H.; Goss, D. J. A Mutant of Eukaryotic Protein Synthesis Initiation Factor EIF4EK119A Has an Increased Binding Affinity for Both M7G Cap Analogues and EIF4G Peptides. *Biochemistry* **2005**, *44* (11), 4546–4550. https://doi.org/10.1021/bi047645m.

(89) Keiper, B. D.; Gan, W.; Rhoads, R. E. Protein Synthesis Initiation Factor 4G. *Int. J. Biochem. Cell Biol.* **1999**, *31* (1), 37–41. https://doi.org/10.1016/S1357-2725(98)00130-7.

(90) Merrick, W. C.; Pavitt, G. D. Protein Synthesis Initiation in Eukaryotic Cells. *Cold Spring Harb. Perspect. Biol.* **2018**, *10* (12), a033092. https://doi.org/10.1101/cshperspect.a033092.

(91) Liu, Y.; Chin, J. M.; Choo, E. L.; Phua, K. K. L. Messenger RNA Translation Enhancement by Immune Evasion Proteins: A Comparative Study between EKB (Vaccinia Virus) and NS1 (Influenza A Virus). *Sci. Rep.* **2019**, *9* (1), 11972. https://doi.org/10.1038/s41598-019-48559-6.

(92) Liu, Y.; Chia, Z. H.; Liew, J. N. M. H.; Or, S. M.; Phua, K. K. L. Modulation of MRNA Translation and Cell Viability by Influenza A Virus Derived Nonstructural Protein 1. *Nucleic Acid Ther.* **2018**, *28* (3), 200–208. https://doi.org/10.1089/nat.2017.0712.

(93) Shen, Q.; Cho, J.-H. The Structure and Conformational Plasticity of the Nonstructural Protein 1 of the 1918 Influenza A Virus. *Biochem. Biophys. Res. Commun.* **2019**, *518* (1), 178–182. https://doi.org/10.1016/j.bbrc.2019.08.027.

(94) Siddiqui, N.; Tempel, W.; Nedyalkova, L.; Volpon, L.; Wernimont, A. K.; Osborne, M. J.; Park, H.-W.; Borden, K. L. B. Structural Insights into the Allosteric Effects of 4EBP1 on the Eukaryotic Translation Initiation Factor EIF4E. *J. Mol. Biol.* **2012**, *415* (5), 781–792. https://doi.org/10.1016/j.jmb.2011.12.002.